Comparative study of machine learning-based multi-objective prediction framework for multiple building energy loads

X.J. Luo, Lukumon O. Oyedele*, Anuoluwapo O. Ajayi and Olugbenga O. Akinade

Big Data Enterprise and Artificial Intelligence Laboratory
University of the West of England, Frenchay Campus, Bristol, United Kingdom
*Corresponding author: l.oyedele@uwe.ac.uk

Abstract

Buildings are one of the significant sources of energy consumption and greenhouse gas emission in urban areas all over the world. Lighting control and building integrated photovoltaic (BIPV) are two effective measures in reducing overall primary energy consumption and carbon emission during building operation. Due to the complex energy nature of the building, accurate day-ahead prediction of heating, cooling, lighting loads and BIPV electrical power production is essential in building energy management. Owing to the changing metrological conditions (i.e. outdoor air dry-bulb temperature, relative humidity, solar radiation and cloud cover), diversity and complexity of buildings, building energy load demands and BIPV electrical power production is highly variable. This may lead to poor building energy management, extra primary energy consumption or thermal discomfort. In this study, three machine learning-based multi-objective prediction frameworks are proposed for simultaneous prediction of multiple energy loads. The three machine learning techniques are artificial neural network, support vector regression and long-short-term-memory neural network. Since heating, cooling, lighting loads and BIPV electrical power production share similar affecting factors such as weather data and building operating schedules, it is computational time saving to adopt the proposed multi-objective prediction framework to predict multiple building energy loads and BIPV power production. To further assess the robustness of three proposed predictive models, they are tested with different heat transfer coefficients of windows and walls, as well as window-to-wall ratios. The mean absolute percentage error of the three proposed predictive models for all cases is less than 10%. The ANN-based predictive model results in the smallest mean absolute percentage error while SVM-based one cost the shortest computation time.

Keywords

Prediction framework; Artificial neural network; Support vector machine; Long-short-term-memory; Multiple energy loads; Building integrated photovoltaic.

1. **Introduction**

Building operations accounted for 30% of global final energy consumption and 28% of energy-related carbon dioxide emissions in 2017 [1]. Global final energy consumption in buildings increased by 5% between 2010-2017, while the emission appeared to have levelled off. Utilization of renewable energy and adoption of effective energy management are two promising approaches in reducing global final energy consumption and help the building sector become carbon natural in the long term. Generally, lighting contributes to approximately 17% of the building electricity consumption [2]. Artificial lighting should be reduced when daylight is sufficient [3]. As the internal heat gain, lighting also impacts the overall building heating and cooling loads [4]. Meanwhile, solar energy is generally considered as the most reliable energy source in nature, thus building integrated photovoltaic (BIPV) can be equipped to convert solar energy into electricity. In a nutshell, lighting control and BIPV are two effective measures for improving building energy efficiency. With the adoption of lighting control and BIPV, the energy nature of the building would become more comprehensive. However, the effective building energy management relies on the accurate and reliable prediction of building energy load demands and BIPV electrical power production.

1.1 Literature review

The utilization of photovoltaics (PV) has been continuously growing within the power sector and shows a phenomenal increase among all renewable energy sources over the last five years [5]. In particular, BIPV systems are one of the most promising applications of solar power technologies, which offer considerable potential in reducing building energy consumption. Wessam *et al.* [6] proposed a regression tree-based predictive model for probabilistic forecast of electrical power generation of a rooftop PV system. Marcelo *et al.* [7] proposed a quantile regression forests-based predictive model for PV power production of different PV plants. Joao *et al.* [8] proposed a hybrid principal component analysis and support vector regression-based predictive model for PV power production within a regional scale. The above-mentioned three predictive models were all trained using the historical measurements of the real PV systems and weather data. However, the independent PV systems (rooftop PV panel, PV plants and regional PV systems) were considered, while the interactive effects of PV panel with the building façade was not accounted. Gao *et al.* [9] compared the performance of the artificial neural network (ANN), genetic programming, and adaptive neuro-fuzzy inference system in predicting the thermal and electrical performance of BIPV. The effects of different design parameters (i.e. duct length, width, depth and air mass flow rate) on the performance of BIPV were evaluated. Juwel *et al.* [10] adopted the SVM algorithm for forecasting the electrical power output of BIPV. The input datasets to the predictive model were the mass flow rate, inlet and outlet temperature of the working fluid as well as the BIPV surface temperature. Abdulwahab *et al.* [11] used the ANN algorithm

to estimate the thermodynamic performance of the BIPV system. The input datasets to the predictive model included the geometry design (i.e. length, depth and width of the channel) and air mass flow rate. However, these three BIPV power predictive models were based on a certain value of solar radiation and were generally used for system design purposes.

To investigate the relationship between sunlight availability and active occupancy with lighting, Palacios *et al.* [12] proposed a bottom-up stochastic predictive model for lighting's electricity consumption in the residential sector. Meanwhile, Kadir *et al.* [13] adopted the SVM-based predictive model to forecast the daily lighting energy consumption in the office building. Daily average sky cover and day type are the input datasets to the SVM algorithm. These two studies are effective at daily lighting electricity consumption.

Accurate prediction of multiple energy loads is indispensable in energy system scheduling and supply-side management [14, 15]. The building heating load was generally estimated based on the load demand of district heating systems [16-19] or water source heat pumps (WSHP) [20, 21], the cooling demand was evaluated according to the load demand of chilled water systems [22-25] or HVAC systems [26-34], while the electricity demand was assessed using the electricity consumption of the building [35-50]. For building energy loads prediction, the data-driven predictive models were generally trained using the historical building operating data. Through the training process, parameters of the predictive models could be obtained to reveal the complex relationship between the input and output datasets. The widely used machine learning algorithms in building energy load prediction contain multiple-linear regression (MLR) [20, 21, 25, 45], Gaussian process regression (GPR) [20], various artificial neuron network (ANN) algorithms [16, 20-23, 25-27, 35, 38, 39, 42-44, 47], support vector machine (SVM) algorithms [7-19, 23-25, 28, 32-35, 37, 43, 44, 48] and deep learning algorithms [29, 31, 36, 41, 44, 49, 50]. The commonly adopted input datasets to the predictive models include the outdoor air dry-bulb temperature, outdoor air wet-bulb temperature, outdoor air relative humidity, wind speed, relative humidity, solar radiation and historical load demands.

Table 1. Summary of literature review.

Ref	Input dataset	Prediction objectivity	Prediction algorithm	Application area
6	Cloudiness, dew point, humidity, pressure, ambient temperature, wind direction, wind speed	PV Electrical power	Regression tree	Rooftop PV panel
7	Ambient temperature, relative humidity, wind speed, wind direction, solar radiation and precipitation		Extreme learning machine	PV Plants
8	Air temperature, air relative Humidity, cloudiness, solar irradiance		Principal component analysis and SVM	Regional scale
9	Geometry design of PV system (i.e. Length, depth and width of the channel) and air mass flow rate		ANN, adaptive neuro-fuzzy inference system	BIPVT system
10	Mass flow rate, inlet and outlet temperature of the working fluid as well as the BIPV surface temperature		SVM	BIPV system
11	Geometry design (i.e. Length, depth and width of the channel) and air mass flow rate		ANN	BIPV system
12	Sunlight availability and active occupancy	Lighting energy consumption	Stochastic models	Residential
13	Daily average sky cover and day type		SVM	Office building
16	Outdoor air dry-bulb temperature, wind speed, solar radiation, relative humidity, heating consumption of the previous day	Heating load of district heating system	ANN and adaptive neuro-fuzzy inference system	University campus
17	Outdoor air dry-bulb temperature, primary/return chilled water temperature, flow rate		SVM with discrete wavelet transform	District scale
18	Outdoor air dry-bulb temperature and heating load at previous time step		SVM with different kernels	District scale
19	Heat load data, outdoor temperature, primary supply/return temperature, and flow rate		SVM with firefly algorithm	District scale
20	Outdoor dry-bulb temperature, wet-bulb temperature, solar radiation, wind speed	Heating load of WHSP	MLR, GPR and ANN	Office premises
21	Wet-Bulb Temperature, Dry-Bulb Temperature, Wind Direction, Solar Radiation, Dew Point Temperature, and Wind Speed		Regression tree, GPR, MLR and ANN	Office premises
22	Outdoor dry-bulb temperature, wet-bulb temperature, temperature of water leaving the chiller	Cooling load of chilled water system	ANN	Office building
23	Outdoor dry-bulb temperature, solar radiation, occupancy		ANN, SVM	Office building
24	Direct normal radiation and diffuse horizontal radiation, dry bulb temperature, relative humidity, wind direction and wind speed.		Wavelet-partial least squares regression-SVM model	Office building
25	Outdoor dry-bulb temperature, relative humidity, wind direction and speed, outdoor luminance		MLR, regression tree, SVM, DNN	Educational building
26	Historical cooling loads, ambient air temperature, solar radiation and room temperature setpoint	Cooling load of HVAC system	ANN with ensemble approach	HVAC in office building
27	Wet-Bulb Temperature, Dry-Bulb Temperature, Wind Direction, Solar Radiation, Dew Point Temperature, and Wind Speed.		ANN	Institutional building
28	Outdoor dry-bulb temperature, relative humidity and global horizontal solar radiations		Wavelet decomposition-SVM	Office building
29	Outdoor temperature, indoor temperature, energy demand from the last time step and solar irradiance Q		LSTM	Office building
30	Dry-bulb temperature, relative humidity		Takagi-Sugeno fuzzy	City scale
31	Weather data, time of day, and previous consumption.		LSTM	Library
32	Temperature of supply air, return air and fresh air		Rough set-based SVM	Office building
33	Temperature, relative humidity and solar radiation		SVM	Office building
34	Historical cooling load		Chaos–SVM, wavelet decomposition-SVR	Commercial building
35	Temperature, global irradiance, humidity, wind velocity, weekday Index	Electricity consumption	MLR, ANN, DNN SVM	Administration building

36	Time series electricity consumption		LSTM	Residential
37	Temperature, relative humidity, solar radiation		SVM	Hotel building
38	Dry-bulb/wet-bulb temperature, solar radiation clearness index, building envelope designs		ANN	Office building
39	Historical load, day of the week, type of the day, hour of the, temperature, humidity, and wind speed		ANN, Autoregressive Integrated Moving Average	Commercial building
40	Historical electricity consumption		Random forest	Multiple
41	Cooling degree-days, total heated area, household income, dwelling type		DNN	Residential buildings
42	Temperature, moisture content, relative humidity, solar radiation, previous electricity consumption		C-means clustering based ANN	Office buildings
43	Dry-bulb/dew-point temperature, relative humidity, pressure, cloud, rainfall, solar radiation, evaporation		Ensemble of MLR, SVR, MLP	Office building
44	Historical electricity consumption		SVM, ANN, RNN and LSTM	City scale
45	Outdoor air temperature, humidity ratio, wind speed, diffuse solar radiation, direct solar radiation		MLR, Gaussian mixture regression	Office building
46	Wind speed, solar radiation, humidity ratio, and outdoor dry-bulb temperature		Teaching learning based optimization	Office building
47	Temperature, humidity, working day		ANN	A shopping mall
48	Dew point temperature, wind direction, wind velocity, outdoor temperature, precipitation intensity and quantity, relative humidity, working time schedule		SVM	District scale
49	Weather information time of the day, holiday		CNN	District scale
50	Historical electricity consumption		RNN	Commercial/residential building

1.2 Research gaps and Contribution

The feasibility of adopting various machine learning approaches in prediction of BIPV power, lighting consumption, thermal load demand and electricity consumption were investigated in the literature review. The input dataset, prediction objectivity, prediction algorithms and application area is summarized in Table 1. It is found that various machine learning techniques, such as MLR, ANN, SVM and deep learning algorithms, were identified effective in predicting various energy consumption and load demands. However, the following deficits are identified in the literature review:

- The prediction models for hourly PV power production were developed for a single PV power plant or system. There is a lack of study considering the variation of PV power production due to the changing thermal performance of building envelop;
- In those BIPV electrical power predictive models, the prediction was conducted at the design stage with the fixed value of solar radiation. However, the hourly BIPV power output should be variable due to changing weather and building thermal conditions. There is a lack of study regarding the prediction of variable hourly BIPV electrical power production;
- In those lighting load studies, daily total lighting load was predicted according to the daily average value of cloud cover and solar radiation. Nevertheless, the hourly lighting load should be variable

due to the changing cloud cover and solar radiation. There is a lack of study regarding the prediction of a variable hourly lighting load;

- In those heating, cooling and electricity load studies, the conventional office or residential buildings were set as the reference building. There has been very little work on predicting energy load demands with the adoption of BIPV system and lighting control in buidlings.
- Most of the above-mentioned building energy predictive models were of single-objective, such as heating, cooling or electricity load. There is a lack of study predicting a set of different objectives. Hence, it may be not able to provide sufficient insights into the complex energy nature of sustainable buildings.

In view of the above-discussed research gaps, this paper aims to propose a novel multi-objective prediction framework for multiple building energy load demands and electrical power production. The proposed multi-objective predictive model will have the following unique features:

- The target building is adopted with BIPV system and lighting control, which has comprehensive energy nature;
    - The heating, cooling, lighting loads and BIPV electrical power output would be predicted simultaneously;
- The variable hourly BIPV electrical power production would be predicted according to the changing weather data and building thermal performance;
- The variable hourly lighting load would be predicted based on the changing cloud cover and solar radiation.

Therefore, the present paper aims to leverage the latest developments in big data and machine learning to create a multi-objective predictive model with the predicting capabilities of hourly heating, cooling, lighting loads and BIPV electrical power production. This research will provide the foundation for building management system, designing supply and demand-side management as well as constructing fault detection and diagnosis strategies.

The rest of the paper is structured like this: the next section discusses the mathematical models of the building with daylighting control and BIPV. The third part illustrates the structure of the historical database. The fourth part presents the three proposed predictive models. The fifth part evaluates the prediction results. The sixth part expresses the implication for practice and future direction while the last section provides the conclusion and main features identified from the study.

2. **Building with daylighting control and BIPV**

To investigate the effects of lighting control and BIPV on building energy loads, thermal models are developed for four different cases of building: without BIPV and without daylighting control (nBnL), with BIPV but without daylighting control (BnL), without BIPV but with daylighting control (nBL), as well as with BIPV and daylighting control (BL). The detailed building information, the thermal model of the building, lighting control algorithm and BIPV model are discussed in this section.

2.1 Building information

A generic building is adopted as a baseline reference for the following comparison and evaluation. The generic building is incorporated with most of the design features commonly identified in office buildings in the UK. The detailed information can be found in Ref. [51-53]. Briefly, the baseline reference building is a rectangle (32 m × 16 m) 4-storey office block with curtain wall designs and a centralized HVAC system. The floor-to-floor distance is 3.5 m. The 4 floors share the same floor plan, and each floor is divided into three zones: zone 1A, zone 1B and zone 2. Zones 1A and 1B are the office rooms while zone 2 serves as the corridor. The windows are distributed on the north, west and east-sided walls, with the window-to-wall ratio of 50%. For building cases with BIPV (i.e. BnL and BL), the BIPV is installed on the south-faced walls of zone 1A on each floor. The focus of this study is on the building with both BIPV and lighting control (i.e. BL). To keep it consistent, there are no windows on the south-faced walls of buildings without BIPV (i.e. BnL and nBnL).

The three-dimensional view of the baseline building is presented in Fig. 1, with Fig. 1(a) showing the south and west façade, while Fig. 1(b) demonstrating the north and east façade. The front and top views of the baseline reference building are shown in Figs. 2 and 3, respectively. On weekdays, the pre-set schedules of occupant, lighting and office equipment are presented in Fig. 4, while the heating and cooling temperature set-points are shown in Fig. 5. In the legend of Fig. 5, the subscript 1 represents the zones 1A and 1B, while 2 stands for zone 2; *h* and *c* stands for heating and cooling, respectively. On weekends, the building schedules and temperature set points are equal to those at non-working hours (i.e. 1^{st} -6^{th} h, and 19^{th} -24^{th} h) on weekdays. The building envelop materials are adopted as in the guideline [51] while the heat transfer coefficients of external wall, roof, ground and windows are summarized in Table 2. The design criteria of the indoor environment are summarized in Tables 3.

Table 2. Heat transfer coefficients of building envelop.

Building envelop	External wall	Roof	Ground	Window
Heat transfer coefficients (W/m^2 K)	1.517	0.14	0.14	1.51

Table 3. Design criterion of the indoor environment.

Design items		Criteria
Floor area per person (m²/person)	Zones 1A and 1B	14
	Zone 2	8
Lighting heat gain (W/m^2)	Zones 1A and 1B	12
	Zone 2	3.4
Office equipment heat gain (W/m^2)	Zones 1A and 1B	10
	Zone 2	2
Fresh air (L/s/person)		10
Occupant heat gain (W/person)		150
Infiltration		0.3

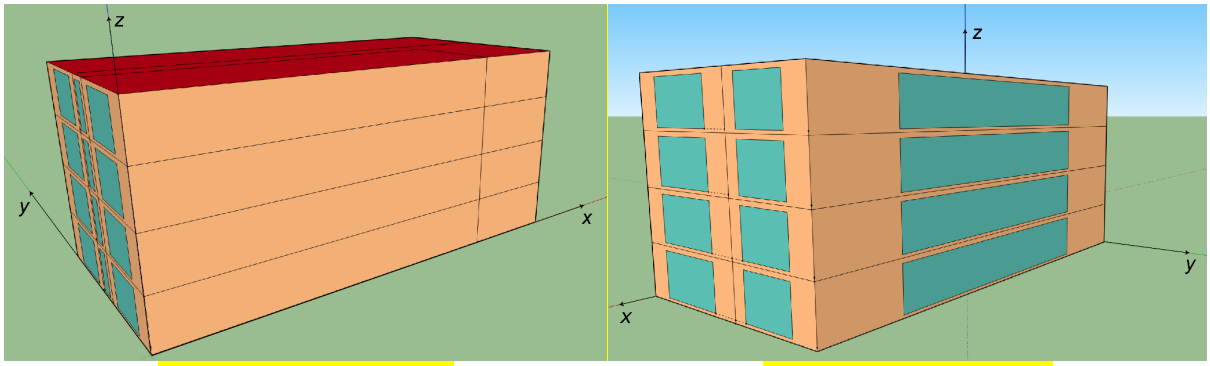

(a)South and west facade (b)North and east facade

Fig. 1. 3D view of the office building

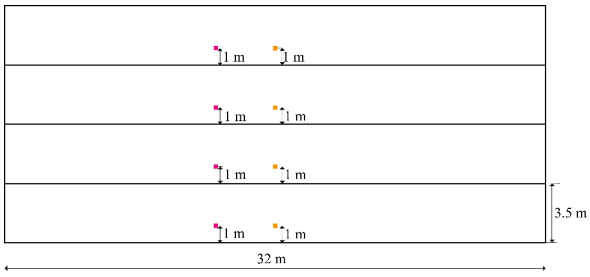

Fig. 2. Front view of the building.

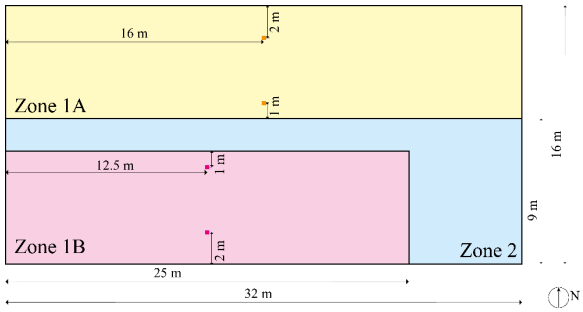

Fig. 3. Top view of the building.

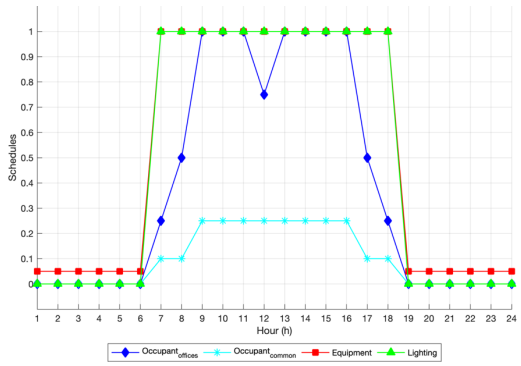

Fig. 4. Operating schedules.

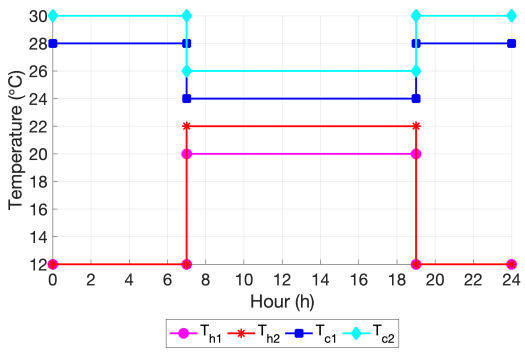

Fig. 5. Temperature set points.

2.2 Thermal model of the office building

Thermal load means the total heat that required to be removed from the building in order to bring it to the indoor design condition as shown in Fig. 4 [54], which include external and internal heat gains.

2.2.1 External heat gain

External heat gains contain convective heat gain through walls Q_{wa}, convective and solar heat gain through windows Q_{wi}, infiltration heat gain Q_{inf} due to air infiltration through the doors and windows as well as ventilation heat gain Q_{ven} owing to forced ventilation for fresh air requirement:

$$Q_{wa} = U_{wa} A_{wa} CLTD_{wa} \quad (1)$$

$$Q_{wi} = U_{wi} A_{wi} CLTD_{wi} + A_{wi} \times G \times SHGF \times SC \quad (2)$$

$$Q_r = U_r A_r CLTD_r \quad (3)$$

$$Q_g = U_g A_g CLTD_g \quad (4)$$

$$Q_{inf} = \rho_a V C_{p,a} ACH_{inf} (T_{db,oa} - T_{db,ia})/3600 + q_{vap} V \rho_a ACH_{inf} (\omega_{oa} - \omega_{ia}) \quad (5)$$

$$Q_{ven} = \rho_a C_{p,a} v_{ven} (T_{db,oa} - T_{db,ia}) + q_{vap} \rho_a v_{ven} (\omega_{oa} - \omega_{ia}) \quad (6)$$

where,

U_{wa} U_{wi} U_r U_g: heat transfer coefficient of walls, windows, roof and ground, respectively (W K^{-1} m^{-2})

A_{wa} A_{wi} A_r A_g: surface areas of walls windows, roof and ground, respectively (m^2)

$T_{db,oa}$ and $T_{db,ia}$: outdoor and indoor air dry-bulb temperature (K)

G: global solar radiation (W m^{-2})

$CLTD_{wa}$ and $CLTD_{wi}$: cooling load temperature differences of walls and windows, respectively (K), which depends on $T_{db,oa}$ and $T_{db,ia}$, G, solar time, latitude and month correction

$SHGF$: solar heat gain factor

SC: shading coefficient of the window

ρ_a: density of air (kg m^{-3})

V: volume of thermal zone (m^3)

$C_{p,a}$: specific heat of air (J kg^{-1} K^{-1})

ACH_{inf}: air change per hour due to infiltration (h^{-1})

q_{vap}: latent heat of air vaporization (J kg^{-1})

ω_{oa} and ω_{ia}: humidity ratio of outdoor and indoor air (kg kg^{-1})

v_{ven}: volumetric flow rate due to fresh air ventilation (m^3 s^{-1})

Therefore, external thermal gain mainly depends on the outdoor air dry-bulb temperature $T_{db,oa}$, outdoor air humidity ratio ω_{oa}, global solar radiation G, heat transfer coefficient of walls U_{wa}, windows U_{wi}, roof

U_r and ground U_g, surface areas of walls A_{wa}, windows A_{wi}, roof A_r and ground A_g, as well as the design conditions summarized in Table 3.

2.2.2 Internal heat gain

Internal heat gains are caused by occupants Q_o, lighting Q_l and office equipment (i.e. computers, printers, fax machines and copiers) Q_e, which are mainly determined by the corresponding internal load densities and loading schedules.

$$Q_o = (q_{o,sen} + q_{o,lat}) \times N_o \quad (7)$$

$$Q_l = P_l \quad (8)$$

$$Q_e = P_e \quad (9)$$

where,

$q_{o,sen}$: sensible heat gain per person (W person^{-1})

$q_{o,lat}$: latent heat gain per person (W person^{-1})

N_o: quantity of occupants (person)

P_l: electrical power consumption of lighting (W)

P_e: electrical power consumption of office equipment (W)

2.2.3 Heating and cooling loads

Heating load Q_h and cooling load Q_c are determined by the sum of various heat gains discussed above:

if $Q_{wa} + Q_{wi} + Q_r + Q_g + Q_o + Q_l + Q_e + Q_{inf} + Q_{ven} > 0$ **then**

$Q_c = Q_{wa} + Q_{wi} + Q_r + Q_g + Q_o + Q_l + Q_e + Q_{inf} + Q_{ven}$

fi

if $Q_{wa} + Q_{wi} + Q_r + Q_g + Q_o + Q_l + Q_e + Q_{inf} + Q_{ven} < 0$ **then**

$Q_h = Q_{wa} + Q_{wi} + Q_r + Q_g + Q_o + Q_l + Q_e + Q_{inf} + Q_{ven}$

fi

2.3 Lighting control

When daylighting control is not adopted (i.e. for cases nBnL and BnL), artificial lighting is implemented as scheduled in Fig. 4. When daylighting control is adopted (i.e. for cases nBL and BL), DAYSIM can be used to simulate the daylighting control and determine lighting power consumption [55]. Through coupling global solar radiance with daylight coefficient, DAYSIM can be used to calculate the

illuminance profile. In other words, in each thermal zone, a set of daylight coefficients are computed and adopted to determine the internal illuminance at sensor points with a variable sky luminance distribution. Upon determining the daylighting availability, DAYSIM can compute the electrical power consumption of artificial lighting when daylight is not sufficient. The lighting power obtained from DAYSIM is also used in Eq. (6) to determine the lighting heat gain. There are two sensors in each zone 1A and 1B, which are located at the middle point of the *x* direction. One of the sensors is located 2 m from the external wall while the other one is situated 1 m from the internal wall, as shown in Fig. 3. On each floor, the sensors are installed on 1 m from the floor, as shown in Fig. 2. The daylighting control set points are summarized in Table 4.

Table 4. Daylighting control set points.

Minimum input power fraction for continuous dimming control	0.2
Minimum light output fraction for continuous dimming control	0.2
1st illuminance setpoint for switching lighting off	500 lux
2nd illuminance setpoint for switching lighting on	300 lux

2.4 BIPV model

The BIPV is installed on the south-faced walls of zones 1A on each floor. The mathematical model of BIPV is illustrated as Eqs (10-17), while its design parameters are summarized in Table 5.

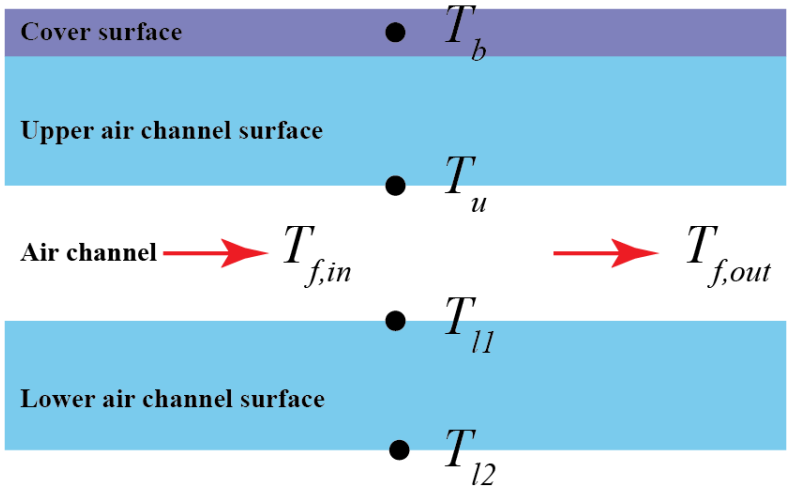

Fig. 6. Schematic diagram of BIPV.

The electrical power production from the BIPV Q_b is determined:

$$Q_b = A_b\ \alpha_b\ G_T\ \eta_b \tag{10}$$

$$\eta_b = \eta_{b,N}\,[1+\varepsilon_T\,(T_b - T_{ref})]\,[1+\varepsilon_G\,(G_T - G_{ref})] \tag{11}$$

where,

η_b: electrical efficiency of BIPV, and:

T_b: temperature of BIPV (K), and is determined through Eqs. (12-15)

$$h_{conv,co}\left(T_b - T_{db,oa}\right) + h_{rad,co}(T_b - T_s) + \frac{T_b - T_u}{g_u} = a_b G_T (1 - h_b) \quad (12)$$

$$h_{conv,f}\left(T_f - T_u\right) + h_{rad,u-l}(T_{l1} - T_u) = \frac{T_b - T_u}{g_u} \quad (13)$$

$$m_f C_{p,f}(T_{f,out} - T_{f,in}) = h_f\left(T_u - T_f\right) + h_f\left(T_{l1} - T_f\right) \quad (14)$$

$$h_f\left(T_f - T_{l1}\right) + h_{rad,u-l}(T_u - T_{l1}) = \frac{T_{l2} - T_{l1}}{g_l} \quad (15)$$

$$\varepsilon_s = 0.711 + 0.005\left(\frac{T_{dp}}{100}\right) + 7.3 \times 10^{-5}\left(\frac{T_{dp}}{100}\right)^2 + 0.013\cos\left(2\pi\frac{t}{24}\right) \quad (16)$$

$$T_s = T_{db,oa}(\varepsilon_s + 0.8(1 - \varepsilon_s)\xi)^{0.25} \quad (17)$$

where,

$h_{rad,co}$: radiative heat transfer coefficient of the cover surface and channel surface (W K^{-1} m^{-2})

$h_{rad,u-l}$: radiative heat transfer coefficient of the channel surface (W K^{-1} m^{-2})

$h_{conv,co}$: convective heat transfer coefficient of the cover surface (W K^{-1} m^{-2})

$h_{conv,f}$: convective heat transfer coefficient of the working fluid (W K^{-1} m^{-2})

m_f: volume flow rate of the working fluid (kg m^{-2} s^{-1})

g_u and g_l: thermal conductivity of the upper and lower air channel surface (K W^{-1} m^{-2})

$C_{p,f}$: specific heat of working fluid (J kg^{-1} K^{-1})

T_{l2}: temperature of the south-side building wall (K)

T_s: sky temperature (K), which is determined by the $T_{db,oa}$, w and the cloud cover ratio ξ.

Table 5. Design parameters of the BIPV [56].

Surface area A_b (m^2)	448
Absorption ratio of BIPV surface α_b	0.8
Emissivity of PV surface	0.9
Substrate resistance (h m^2 K/kJ)	0.01
Channel emissivity	0.9
Back resistance (h m^2 K/kJ)	1.0
Channel height (m)	0.0508
BIPV nominal electrical efficiency $\eta_{b,N}$	0.12
Reference temperature T_{ref} (K)	298
Reference radiation G_{ref} (kJ /h m^2)	3600
Correction coefficient of temperature ε_T	-0.005
Correction coefficient of temperature ε_G	0.000025

3. **Formulation of the database for machine learning-based prediction framework**

For the machine learning-based prediction framework, the input database mainly includes weather profiles, building operating schedules, building thermal performance, while the output dataset is the heating, cooling, lighting loads as well as BIPV power production.

3.1 Generation of database

Owing to the year-round changing weather condition, transient simulation is desired to acquire the yearly profile of heating, cooling, lighting loads and BIPV power production at the time step of one hour. The TRNSYS program is a flexible simulation tool in replicating the transient performance of thermal energy systems, which was developed and is being continuously updated by the Solar Energy Laboratory at the University of Wisconsin since 1975 [57]. The thermal models of building and various energy-related components in TRNSYS have been validated in a variety of studies [58-63]. Therefore, in this study, TRNSYS 18 is implemented as a dynamic simulation platform:

- The built-in Type 56 multi-zone building analytical model can solve the coupled differential equations using matrix inversion techniques and provide a more efficient approach to calculate the interaction between two or more zones. In Type 56, the building envelopes are modelled according to the ASHRAE transfer function approach to determine the heating and cooling loads [64].
- Moreover, TRNSYS 18 also integrates dynamic daylight simulation based on DaySIM into Type 56, in which the 3D geometries of the building model can be used to calculate illuminance levels for sensor points.
- In addition, the built-in component Type 568 is intended to model the BIPV performance. It can be connected with building thermal model Type 56, where Type 56 provides the temperature of the back surface of the BIPV T_{l2} and Type 568 shows the surface temperature of the lower flow channel T_{l1}.

3.2 Characteristics of heating, cooling, lighting loads and BIPV power production

To make the simulation data of heating, cooling, lighting loads and BIPV electrical power output closer to the practical case, the historical weather data recorded at London Heathrow Airport in the years 2017 and 2018 is adopted as inputs to the TRNSYS simulation model. The historical weather data includes outdoor air dry-bulb temperature, outdoor air dew-point temperature, global solar radiation, wind speed and cloud cover ratio.

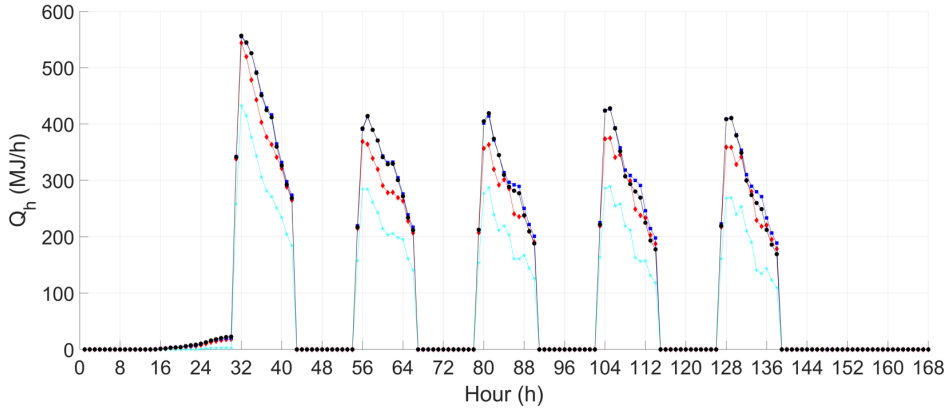

(a) Heating

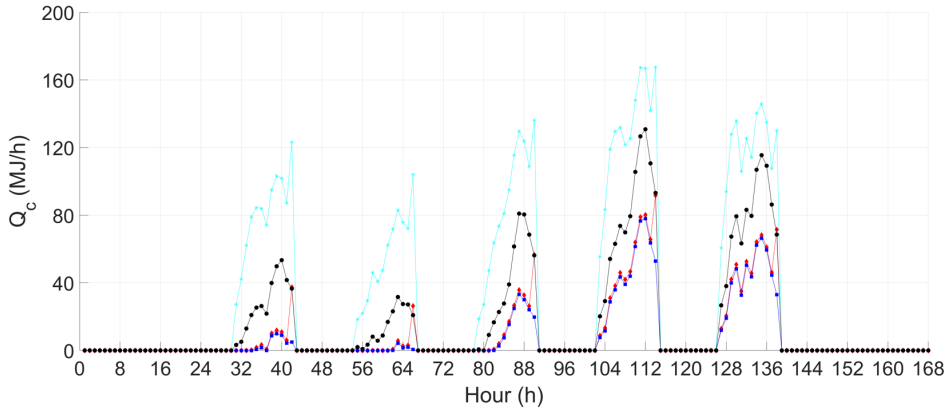

(b) Cooling

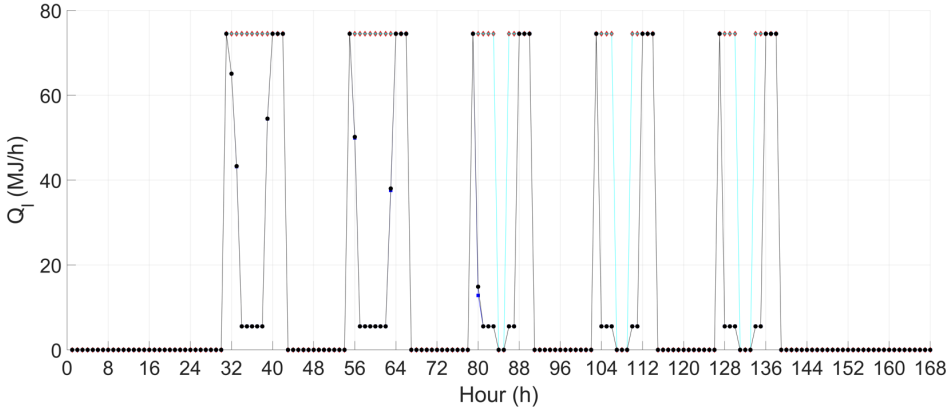

(c) Lighting

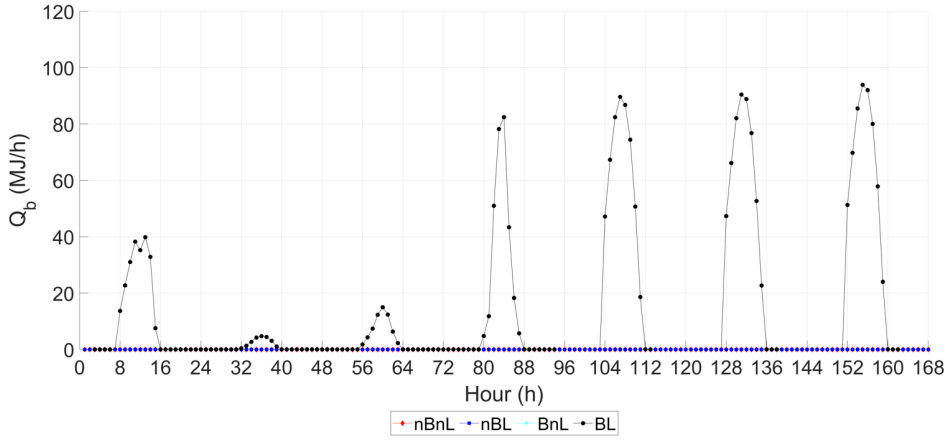

(d) BIPV electrical power

Fig. 7. Energy loads and production of different building types.

To investigate the effects of lighting control and BIPV on the building heating and cooling loads, the peak and year-around total value of heating, cooling, lighting loads and BIPV electrical power production are summarised in Table 6. The heating load, lighting load and BIPV electrical power production of the 2nd week of the year are shown in Figs. 7 (a), (c) and (d), while the cooling load of the 30th week of the year is shown in Fig. 7(b). The trend of heating, cooling, lighting loads and BIPV electrical power production should be similar in each week so the two weeks are selected randomly.

The building heating load with lighting control is larger than that without lighting control. On the contrary, the building cooling load with lighting control is smaller than that without lighting control. It is because that the lighting energy also contributes to the building internal heat load. When the daylight is not sufficient (e.g. the 31st, the 40th - 42nd h of the week), artificial lighting load is at its maximum value to provide sufficient illuminance. However, when the daylight is sufficient (e.g. the 32nd - 39th h of the week), artificial lighting load can be greatly reduced when lighting control is adopted. As a result, 68.4% of the year-round lighting energy consumption can be reduced.

The building heating load with BIPV is smaller than that without BIPV. On the contrary, the building cooling load with BIPV is larger than that without BIPV. It is because that BIPV absorbs a certain amount of solar radiation. With the implementation of BIPV, there exists a peak electrical power production during the middle of each day, while the yearly electrical energy production from the BIPV is 0.3 GJ/m^2.

Table 6. Peak and year-round building energy loads.

	Heating		Cooling		Lighting		BIPV	
	Year-around (GJ)	Peak (MJ/h)	Year-around (GJ)	Peak (MJ/h)	Year-around (GJ)	Peak (MJ/h)	Year-around (GJ)	Peak (MJ/h)
nBnL	325	620	272	218	114	74.5	134	104
nBL	380	670	231	217	42			
BnL	187	510	856	299	114			
BL	344	670	424	280	42			

3.3 Structure of the historical database

Based on the analysis in Section 2, the affecting factors of building energy loads and BIPV electrical power production contain weather data of outdoor air dry-bulb temperature, outdoor air humidity ratio, global solar radiation and cloud cover ratio as well as indoor schedules of occupants, lighting and office equipment. To generate the historical database, these affecting factors, along with indoor air dry-bulb temperature and BIPV temperature at previous 24 hours, as well as heating load, cooling load, lighting load and BIPV electrical power production, are consolidated as database **X** for input variables to the proposed predictive models. Meanwhile, the heating, cooling, lighting loads and BIPV electrical power production at the current time step, are consolidated as database **Z** for output variables expected from

the predictive model. The time step of above-mentioned variables is 1 hour. The data elements in database **X** and **Z** are summarized in Table 7. In this study, the TRNSYS simulation model is developed to represent the real building. Namely, the calculated results of heating, cooling, lighting loads and BIPV power production from the TRNSYS simulation model are taken as the baseline values to compare with the predicted values from the proposed machine learning-based prediction frameworks.

Table 7. Detailed information regarding the historical database.

Variables		This study		Practical application
		Training case	Testing case	Training and testing cases
X	Outdoor air dry-bulb temperature $T_{db,oa,i}$	Weather data in 2017	Weather data in 2018	Weather data recorded at local or weather station
	Outdoor air humidity ratio w_i			
	Global horizontal radiation G_i			
	Cloud cover ratio ξ_i			
	Schedule of occupants in zones 1A and 1B $S_{o1,i}$	Pre-set schedules as shown in Fig. 4.		Recorded building-related data
	Schedule of occupants in zone 2 $S_{o2,i}$			
	Schedule of office equipment $S_{E,i}$			
	Indoor air dry-bulb temperature $T_{db,ia,i-1}$	Simulated building operating data in 2017	Simulated building operating data in 2018	Temperature sensor measurement data
	BIPV temperature at last time step $T_{b,i-1}$			
	BIPV temperature at same time step of last day $T_{b,i-24}$			
	Heating load at the last time step $Q_{h,i-1}$	Simulated building energy data in 2017	Simulated building energy data in 2018	Energy meter measurement data
	Heating load at time step *i*-2 $Q_{h,i-2}$			
	Heating load at time step *i*-3 $Q_{h,i-3}$			
	Heating load at time step *i*-4 $Q_{h,i-4}$			
	Heating load at same time step of last day $Q_{h,i-24}$			
	Cooling load at the last time step $Q_{c,i-1}$			
	Cooling load at time step *i*-2 $Q_{c,i-2}$			
	Cooling load at time step *i*-3 $Q_{c,i-3}$			
	Cooling load at time step *i*-4 $Q_{c,i-4}$			
	Cooling load at the same time step of last day $Q_{c,i-24}$			
	Lighting load at the last time step $Q_{l,i-1}$			
	BIPV power production at the last time step $Q_{b,i-1}$			
Z	Heating load at the current time step $Q_{h,i}$	Simulated energy data in 2017	Simulated energy data in 2018	Energy meter measurement data
	Cooling load at the current time step $Q_{c,i}$			
	Lighting load at the current time step $Q_{l,i}$			
	BIPV power production at current time step $Q_{b,i}$			

In summary, there are N_{in} = 22 input variables and 4 output variables at each time step, while the total time step is N_t = 365 × 24 = 8760. And

$$\mathbf{X} = \begin{bmatrix} x_{1,1} & x_{1,2} & & x_{1,j} & x_{1,N_{in}} \\ x_{2,1} & x_{2,2} & \cdots & x_{2,j} & \cdots x_{2,N_{in}} \\ \cdots & \cdots & \cdots & \cdots & \cdots \\ x_{i,1} & x_{i,2} & \cdots & x_{i,j} & \cdots \\ \cdots & \cdots & \cdots & \cdots & \cdots \\ x_{N_t,1} & x_{N_t,2} & & x_{N_t,j} & x_{N_t,N_{in}} \end{bmatrix}$$

$$\mathbf{Z} = \begin{bmatrix} Q_{h,1} & Q_{c,1} & Q_{l,1} & Q_{b,1} \\ Q_{h,2} & Q_{c,2} & Q_{l,2} & Q_{b,2} \\ \cdots & \cdots & \cdots & \cdots \\ Q_{h,N_t} & Q_{c,N_t} & Q_{l,N_t} & Q_{b,N_t} \end{bmatrix}$$

where, $x_{i,1} = T_{db,oa,i}$, $x_{i,2} = w_i$, $x_{i,3} = G_i$, $x_{i,4} = \xi_i$, $x_{i,5} = S_{o1,i}$ $x_{i,6} = S_{o2,i}$, $x_{i,7} = S_{E,i}$, $x_{i,8} = T_{db,ia,i-1}$, $x_{i,9} = T_{b,i-1}, x_{i,10} = T_{b,i-1}, x_{i,11} = Q_{h,i-1}$, $x_{i,12} = Q_{h,i-2}$, $x_{i,13} = Q_{h,i-3}$, $x_{i,14} = Q_{h,i-4}$, $x_{i,15} = Q_{h,i-24}, x_{i,16} = Q_{h,i-1}, x_{i,17} = Q_{h,i-2}, x_{i,18} = Q_{h,i-3}, x_{i,19} = Q_{h,i-4}, x_{i,20} = Q_{h,i-24}, x_{i,21} = Q_{l,i-1}, x_{i,22} = Q_{b,i-1}$.

4. Machine learning-based prediction framework

The schematic diagram of the three proposed predictive models is presented in Fig. 8. In each predictive model, ANN, SVM or LSTM algorithm is adopted.

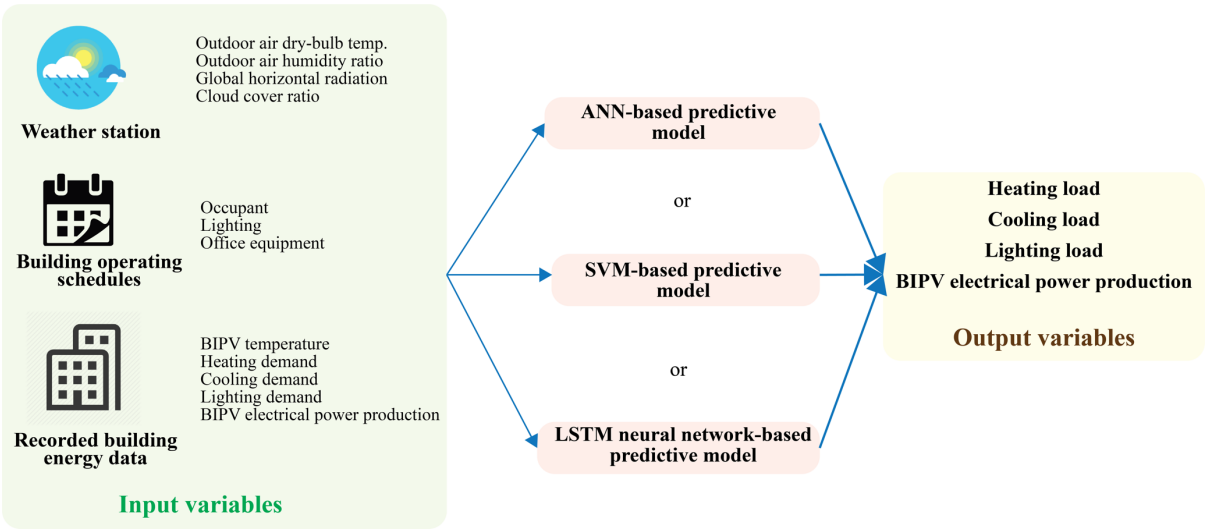

Fig. 8. Schematic diagram of the proposed predictive model

Because the datasets of each parameter do not follow the normal distribution, the min-max scaling approach is adopted to normalize the historical database **X**, for each j:

$$y_{i,j} = \frac{x_{i,j} - \min\limits_{1 \le i \le N_t} x_{i,j}}{\max\limits_{1 \le i \le N_t} x_{i,j} - \min\limits_{1 \le i \le N_t} x_{i,j}} \tag{18}$$

4.1 ANN-based predictive model

The ANN algorithm consists of three layers: the input layer, the hidden layer and the output layer [65]. The elementary component in the ANN algorithm is the artificial neuron which is aligned in layers and connected to neurons in other layers through synaptic weights. The values of the weights are decided through the training process. The diagram of the ANN-based predictive model is shown in Fig. 9. As illustrated in Table 7, there are N_i = 22 input variables $\boldsymbol{Y_j}$ ($j = 1, 2, \ldots, 22$) and 4 output variables ($\boldsymbol{Q_h}$, $\boldsymbol{Q_c}$, $\boldsymbol{Q_l}$ and $\boldsymbol{Q_b}$) to the ANN predictive model:

$$\boldsymbol{Y_j} = [y_{1,j}; y_{2,j}; \ldots; y_{i,j}; \ldots; y_{N_t,j}]$$
$$\boldsymbol{Q_h} = [Q_{h,1}; Q_{h,2}; \ldots; Q_{h,i}; \ldots; Q_{h,N_t}]$$
$$\boldsymbol{Q_c} = [Q_{c,1}; Q_{c,2}; \ldots; Q_{c,i}; \ldots; Q_{c,N_t}]$$
$$\boldsymbol{Q_l} = [Q_{l,1}; Q_{l,2}; \ldots; Q_{l,i}; \ldots; Q_{l,N_t}]$$
$$\boldsymbol{Q_b} = [Q_{b,1}; Q_{b,2}; \ldots; Q_{b,i}; \ldots; Q_{b,N_t}]$$

The quantity of neurons in the hidden layer N is tested within the range {2-50} in view of both algorithm effectiveness and computation time.

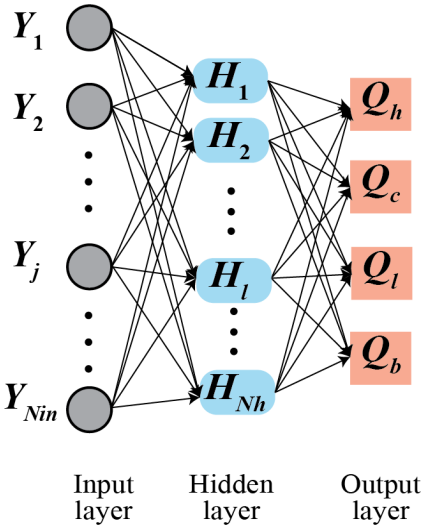

Fig. 9. Diagram of the ANN-based predictive model.

In the ANN-based predictive model, the l^{th} neuron $\boldsymbol{H_l}$ in the hidden layer is defined as:

$$\boldsymbol{H_l} = f\left(\sum_{j=1}^{j=N_{in}} (w_{jl}\boldsymbol{Y_j})\right) \quad (19)$$

where w_{jl} is the weight of the connection of the j^{th} input to the l^{th} neuron, and f is the Sigmoidal transfer function. $\widetilde{\boldsymbol{Q}}_{\boldsymbol{h}}$, $\widetilde{\boldsymbol{Q}}_{\boldsymbol{c}}$, $\widetilde{\boldsymbol{Q}}_{\boldsymbol{l}}$ and $\widetilde{\boldsymbol{Q}}_{\boldsymbol{b}}$ are the predicted heating, cooling lighting loads and BIPV power production, respectively:

$$\widetilde{\boldsymbol{Q}}_{\boldsymbol{h}} = f\left(\sum_{l=1}^{l=N_{hi}}(w_{l1}\boldsymbol{H}_{\boldsymbol{l}})\right) \quad (20)$$

$$\widetilde{\boldsymbol{Q}}_{\boldsymbol{c}} = f\left(\sum_{l=1}^{l=N_{hi}}(w_{l2}\boldsymbol{H}_{\boldsymbol{l}})\right) \quad (21)$$

$$\widetilde{\boldsymbol{Q}}_{\boldsymbol{l}} = f\left(\sum_{l=1}^{l=N_{hi}}(w_{l3}\boldsymbol{H}_{\boldsymbol{l}})\right) \quad (22)$$

$$\widetilde{\boldsymbol{Q}}_{\boldsymbol{b}} = f\left(\sum_{l=1}^{l=N_{hi}}(w_{l4}\boldsymbol{H}_{\boldsymbol{l}})\right) \quad (23)$$

The aim of the training process is to minimize the squared error $E_{D,ANN}$ between predicted energy loads ($\widetilde{\boldsymbol{Q}}_{\boldsymbol{h}}, \widetilde{\boldsymbol{Q}}_{\boldsymbol{c}}, \widetilde{\boldsymbol{Q}}_{\boldsymbol{l}}$ and $\widetilde{\boldsymbol{Q}}_{\boldsymbol{b}}$) and the TRNSYS simulated energy loads ($\boldsymbol{Q}_{\boldsymbol{h}}, \boldsymbol{Q}_{\boldsymbol{c}}, \boldsymbol{Q}_{\boldsymbol{l}}$ and $\boldsymbol{Q}_{\boldsymbol{b}}$):

$$E_{D,ANN} = \sum[(\widetilde{\boldsymbol{Q}}_{\boldsymbol{h}} - \boldsymbol{Q}_{\boldsymbol{h}})^2 + (\widetilde{\boldsymbol{Q}}_{\boldsymbol{c}} - \boldsymbol{Q}_{\boldsymbol{c}})^2 + (\widetilde{\boldsymbol{Q}}_{\boldsymbol{l}} - \boldsymbol{Q}_{\boldsymbol{l}})^2 + (\widetilde{\boldsymbol{Q}}_{\boldsymbol{b}} - \boldsymbol{Q}_{\boldsymbol{b}})^2] \quad (24)$$

Levenberg-Marquardt approach is adopted to minimize $E_{D,ANN}$, thus various weights of the ANN predictive model (i.e. w_{kl}, w_{l1}, w_{l2}, w_{l3} and w_{l4}) can be determined.

4.2 SVM-based predictive model

In SVM algorithm, kernel functions are used to implicitly map the input features in the original low-dimensional input space into a high-dimensional output feature space [66]. The schematic diagram of the SVM predictive model is shown in Fig. 10. The format of input dataset to the SVM-based predictive model is different from that to the ANN-based predictive model. The input dataset is consolidated as $Y_i = [y_{i,1}\ y_{i,2} \ldots\ y_{i,j} \ldots y_{i,N_{in}}]$ and $\mathbf{Y} = [Y_1; Y_2; \ldots; Y_i; \ldots; Y_{N_t}]$. Meanwhile, the output dataset is consolidated as $\widetilde{\mathbf{Q}}_{\mathbf{i}} = [\tilde{Q}_{h,i}\ \tilde{Q}_{c,i}\ \tilde{Q}_{l,i}\ \tilde{Q}_{b,i}]$.

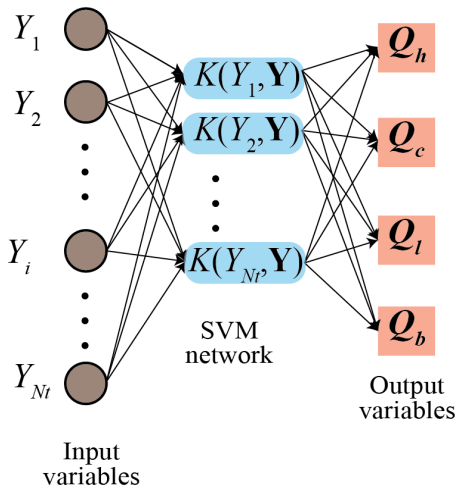

Fig. 10. Diagram of the SVM predictive model.

The principle of SVM is to solve the nonlinear prediction problem in a multidimensional function space via the nonlinear transformation $\varphi(\cdot)$, thus the parameters of the SVM algorithm are determined to fit the relationships between $\mathbf{Y}$ and $\mathbf{Q_i}$:

$$\widetilde{\mathbf{Q}}_\mathbf{i} = f(Y_i) = W \cdot \varphi(Y_i) + b \tag{24}$$

where W and b are the coefficients of the SVM model. The aim of training the SVM predictive model is to determine W and b to minimize the squared error $E_{D,SVM}$ between the prediction result $\widetilde{\mathbf{Q}}_\mathbf{i}$ and TRNSYS simulation result $\mathbf{Q_i}$:

$$E_{D,SVM} = \sum(\mathbf{Q_i} - \widetilde{\mathbf{Q}}_\mathbf{i})^2 \tag{25}$$

4.3 LSTM neural network-based predictive model

LSTM is a special variant of recurrent neural networks. Its learnable gates can modulate the flow of information. The persistent cell state has minimal interactions and provides an easy path for gradient flow during back-propagation [67]. The schematic diagram of the LSTM neural network predictive model is shown in Fig. 11. The input dataset to the LSTM neural network is $Y_i = [y_{i,1}\ y_{i,2} \dots\ y_{i,j} \dots y_{i,N_{in}}]$ while the output dataset is $\widetilde{\mathbf{Q}}_\mathbf{i} = [\tilde{Q}_{h,i}\ \tilde{Q}_{c,i}\ \tilde{Q}_{l,i}\ \tilde{Q}_{b,i}]$, which is the same as those to the SVM algorithm. Taking both algorithm effectiveness and computation time into consideration, the quantity of hidden units is tested within the range {2-20}, while other training parameters are summarized in Table 8.

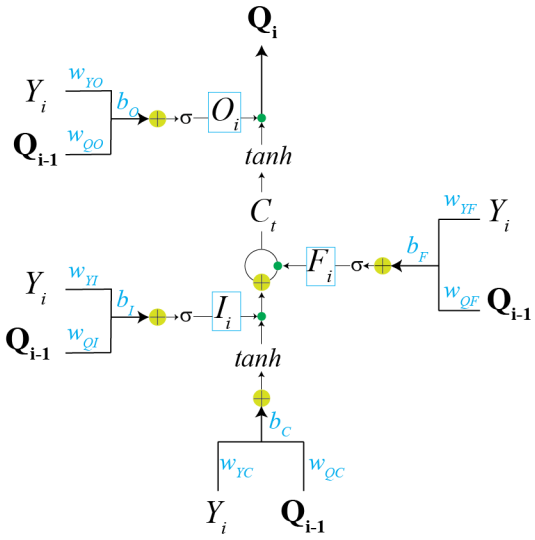

Fig. 11. Diagram of the LSTM neural network-based predictive model.

Table 8. Parameters of LSTM neuron network.

Maximum number of epochs	1000
Size of mini-batch	20
Initial learning rate	0.001
Gradient Threshold	1

There are three gates utilized within an LSTM: input gate I_i, forget gate F_i and output gate O_i: F_i defines the proportion of information to be preserved in C_i. It adopts the sigmoid function as the activation function and outputs a value between zero and one based on Y_i and $\mathbf{Q_{i-1}}$:

$$F_i = sigmoid\ (w_{YF}Y_i + w_{QF}\mathbf{Q_{i-1}} + b_F) \tag{26}$$

where B_F is the bias, w_{YF} and w_{QF} are weight matrices for Y_i and $\mathbf{Q_{i-1}}$, respectively. The input gate I_i defines the proportion of new information to be added for C_i. And:

$$I_i = sigmoid\ (w_{YI}Y_i + w_{QI}\mathbf{Q_{i-1}} + b_I) \tag{27}$$

where b_I is the bias, w_{YI} and w_{QI} are weight matrices for Y_i and $\mathbf{Q_{i-1}}$, respectively. The tanh activation function is then used to create a candidate for updating C_i, and:

$$C_T = tanh\ (F_i{}^{\circ}C_{i-1} + I_i{}^{\circ}(\tanh(w_{YC}Y_i + w_{QC}\mathbf{Q_{i-1}} + b_C))) \tag{28}$$

where ° is the pointwise multiplications, w_{YC} and w_{QC} are weight matrices for Y_i and $\mathbf{Q_{i-1}}$, respectively. The output gate O_i is specified as:

$$O_i = sigmoid\ (w_{YO}Y_i + w_{QO}\mathbf{Q_{i-1}} + B_O) \tag{29}$$

where B_O is the bias, w_{YO} and w_{QO} are weight matrices for Y_i and $\mathbf{Q_{i-1}}$, respectively. The hidden state is calculated as:

$$H_i = O_i{}^{\circ}\ tanh(C_i) \tag{30}$$

Adam optimization is used in determining the various weight matrices (i.e w_{YF}, $w_{QF}, w_{YI}, w_{QI}, w_{YC}, w_{QC}, w_{YO}, w_{QO}$) in the LSTM neuron network [68].

4.4 Performance assessment index

According to Fig. 7, the value range among heating, cooling, lighting load and BIPV power production is quite different. Therefore, the mean absolute percentage error (*MAPE*) is adopted to assess the performance of the proposed three predictive models:

$$MAPE = \frac{1}{N_t}\sum_{i=1}^{i=N_t}\left(\frac{|\tilde{Q}_{h,i}-Q_{h,i}|}{Q_{h,i}} + \frac{|\tilde{Q}_{c,i}-Q_{c,i}|}{Q_{c,i}} + \frac{|\tilde{Q}_{l,i}-Q_{l,i}|}{Q_{l,i}} + \frac{|\tilde{Q}_{b,i}-Q_{b,i}|}{Q_{b,i}}\right) \times 100\% \quad (31)$$

5. Results and discussion

The machine learning-based prediction framework is developed using MATLAB and conducted on a computation tool used for this research is a desktop with a processor of 2.7 GHz Intel Core i5. To evaluate the performance of the proposed machine learning-based multi-objective prediction, its performance for the baseline case is compared to conventional single-objective predictive models. Moreover, to investigate the robustness of the proposed prediction framework, mean absolute percentage error and computational time of each predictive model is assessed at different heat transfer coefficients of windows U_{win}, heat transfer coefficients of walls U_{wall} as well as window-to-wall ratios R_{win}.

5.1 Performance evaluation of the proposed prediction framework

To select the optimal architecture of ANN and LSTM-based predictive model, the quantity of neurons in the hidden layer in ANN and the quantity of hidden units in LSTM is tested in the range {2-50} and {2, 20}, respectively. The result is shown in Fig. 12. It is found that the optimal quantity of neurons in the hidden layer in ANN is 14 while the optimal quantity of hidden units in LSTM is 8.

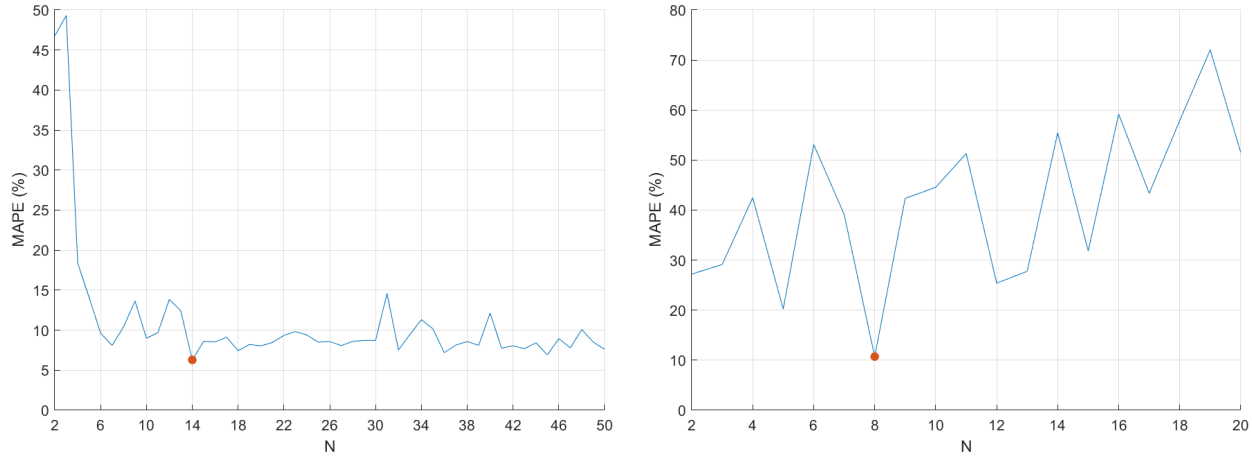

(a) ANN (b) LSTM

Fig. 12. MAPE at different ANN/LSTM architecture.

To investigate the advantage of the proposed multi-objective prediction framework over conventional single-objective prediction model, the conventional single-objective ANN, SVM and LSTM predictive model is developed for heating, cooling, lighting load and BIPV electrical power production, respectively. To keep it consistent, the same input database is adopted in the conventional single-objective ANN, SVM and LSTM model. The prediction performance, represented by *MAPE* value and computational load, is summarized in Table 9.

Table 9. MAPE value and computational time of multi-objective and single-objective predictive models.

Load type	Heating load			Cooling load			Lighting load			BIPV power			Overall		
Performance	MAPE (%)		Time (s)	MAPE (%)		Time (s)	MAPE (%)		Time (s)	MAPE (%)		Time (s)	MAPE (%)		Time (s)
	Train	Test		Train	Test		Train	Test		Train	Test		Train	Test	
m-ANN	N.A.												6.29	8.66	86
m-SVM													9.56	9.70	0.49
m-LSTM													8.52	9.06	2328
s-ANN	6.35	8.54	23	6.19	8.80	26	6.21	8.71	24	6.19	8.57	25	6.24	8.66	98
s-SVM	9.50	9.82	0.14	9.62	9.49	0.14	9.48	9.52	0.13	9.51	9.58	0.15	9.53	9.60	0.56
s-LSTM	8.56	9.01	595	8.49	9.10	601	8.60	9.08	610	8.50	9.02	592	8.54	9.05	2398

Compared to the total computational time (98s, 0.56s and 2398s) of heating, cooling, lighting and BIPV power production from the conventional single-objective ANN, SVM and LSTM-based prediction models, the computational time (86s, 0.49s and 2328s) of the proposed multi-objective prediction model is shorter. The *MAPE* value from the proposed multi-objective prediction framework is similar to that from the conventional single-objective prediction model in both training and testing cases.

It is also found that the multi-objective ANN-based predictive model results in the smallest *MAPE* value with the average computational time; the multi-objective SVM-based predictive model resulted has the largest *MAPE* value with the shortest computational time. On the contrary, the multi-objective LSTM-based predictive model results in the medium *MAPE* value with the longest computational time.

5.2 Evaluation of robustness of the prediction framework

To investigate the robustness of the proposed prediction framework, it is implemented on buildings with different building materials and architectural features. Compared to the building roof, building walls and windows generally occupies larger surface, thus results in larger effects on building thermal performance. Therefore, the different thermal properties of walls, thermal properties of windows and window-to-wall ratios are investigated.

5.2.1 Effect of heat transfer coefficient of windows

The building heating and cooling loads at different heat transfer coefficients of windows (i.e. U_w = 0.74, 1.51 and 2.72 W·m^{-2} K^{-1}) during the 2nd and the 30th week of the year are shown in Fig. 13, while heat transfer coefficient of walls U_{wa} = 1.517 W·m^{-2} K^{-1} and window-to-wall ratio R_{win} = 50%. It is seen that the lower heat transfer coefficient of windows results in lower heating and cooling load.

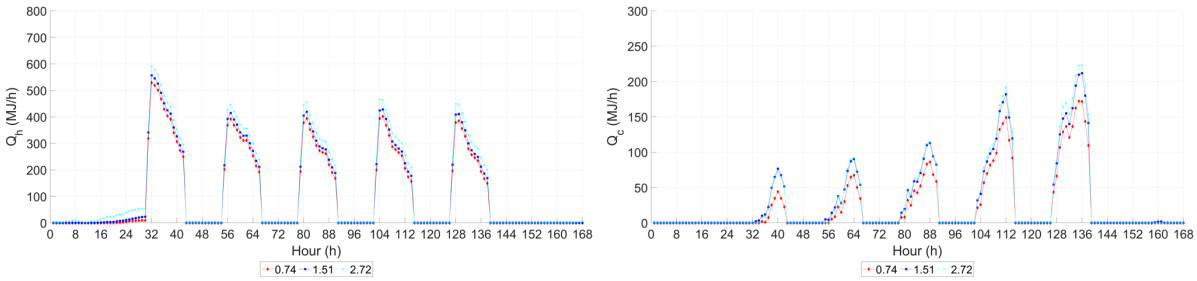

(a) Heating (b) Cooling

Fig. 13. TRNSYS simulated heating and cooling loads at different U_{win}.

The prediction results from two random days in the heating season and cooling season are shown in Fig. 14. Although the heating, cooling, lighting loads and BIPV electrical power production varies among different heat transfer coefficients of windows, the prediction results from the ANN, SVM and LSTM neural network based-predictive models are close to those obtained from the baseline TRNSYS simulation model.

- For heating load prediction, the ANN-based predictive model has the closest result to the TRNSYS simulation model, while the result from LSTM neuron network is closer to the TRNSYS simulation model than that from the SVM model;
- For cooling load prediction, the ANN-based predictive model has the closest result to the TRNSYS simulation model, while the result from SVM model is closer to the TRNSYS simulation model than that from the LSTM neuron network;
- For lighting load prediction, the three proposed predictive models can correctly predict the time-period when the artificial lighting is needed, while there exists a little difference between the predicted heating load values and the TRNSYS simulation results;
- For BIPV electrical power prediction, the results from the ANN-based and SVM-based predictive model are closer to the TRNSYS simulation model than those from the LSTM neuron network-based predictive model.

The *MPE* of the three predictive models for building energy prediction under different heat transfer coefficients of windows is summarized in Table 10. Generally, the *MAPE* of ANN-based predictive model is the smallest, while the *MAPE* of SVM and LSTM neuron network-based predictive models are similar. Moreover, the *MAPE* of testing cases is generally a little larger than that of training cases.

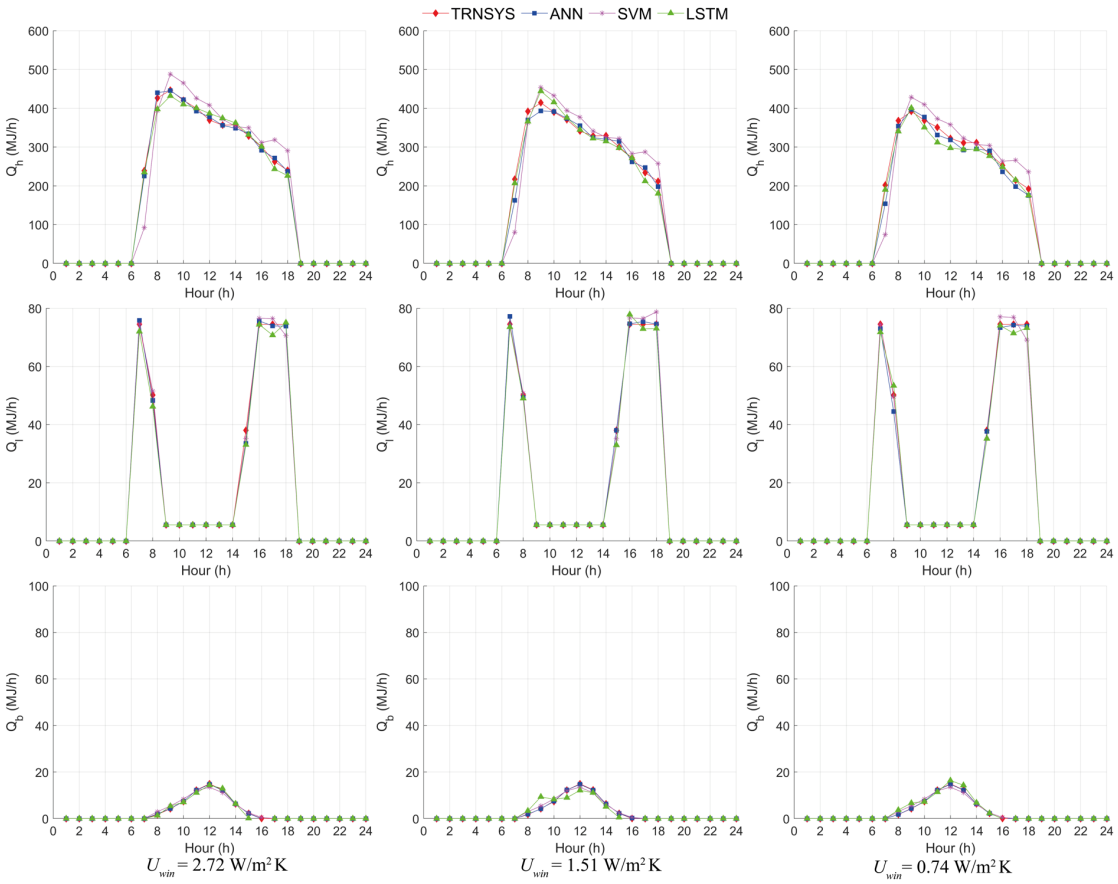

U_{win} = 2.72 W/m²K U_{win} = 1.51 W/m²K U_{win} = 0.74 W/m²K

(a) Training case, heating day

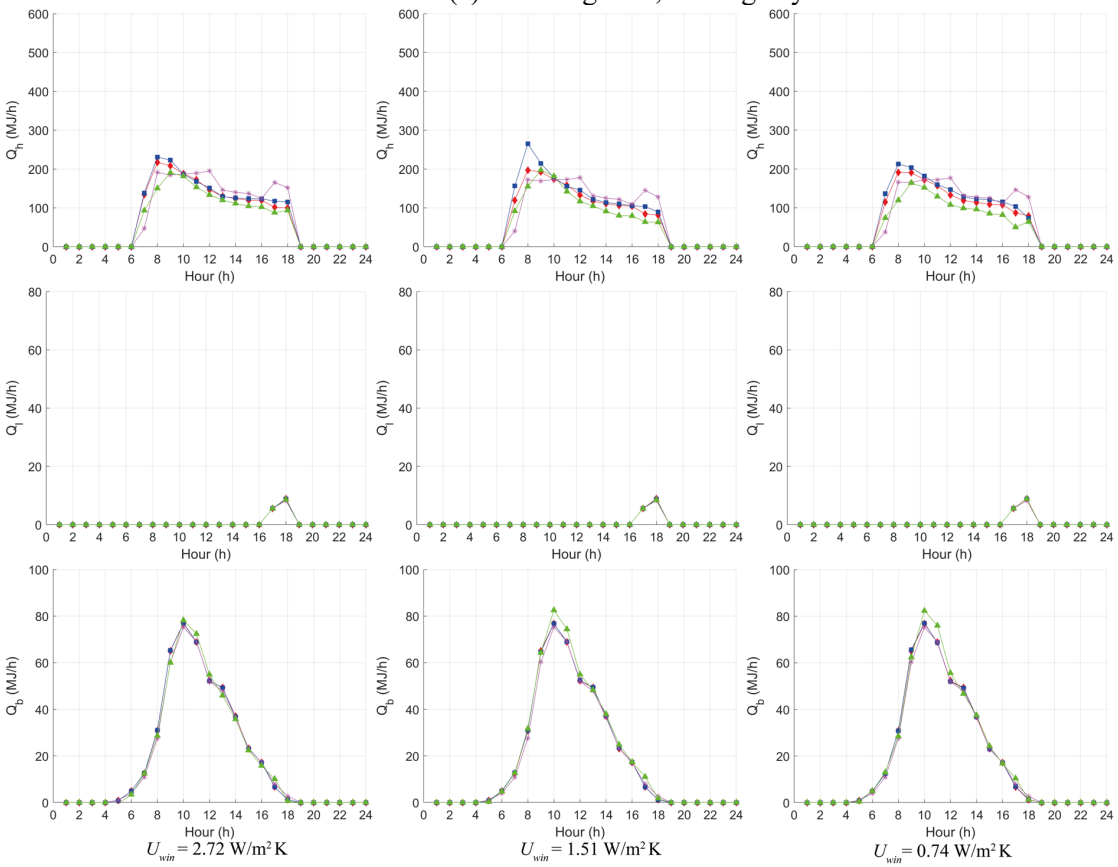

U_{win} = 2.72 W/m²K U_{win} = 1.51 W/m²K U_{win} = 0.74 W/m²K

(b) Testing case, heating day

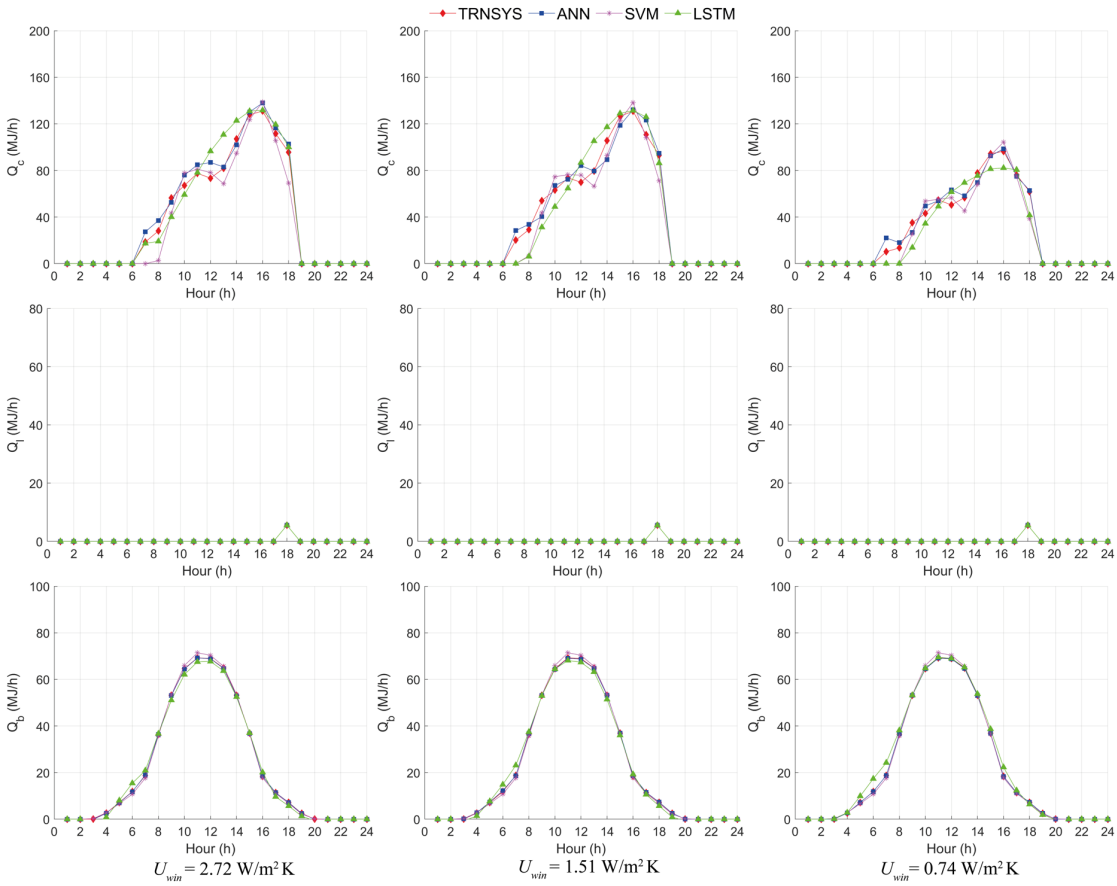

(c) Training case, cooling day

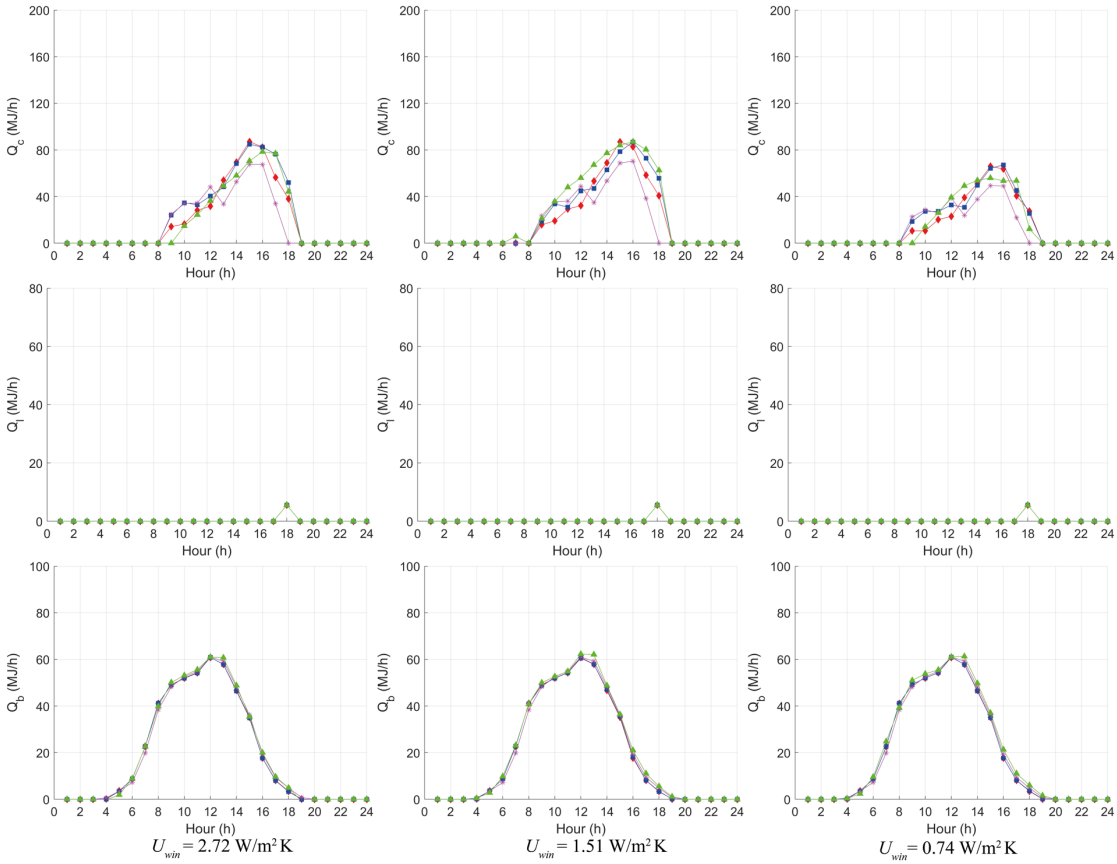

(d) Testing case, cooling day

Fig. 14. Prediction results of building energy loads and BIPV power production at different U_{win}.

Table 10. *MAPE* of prediction results at different heat transfer coefficients of windows.

U_{wa} = 1.517 W·m^{-2} K^{-1}, R_{wi} = 50%			U_{wi} (W·m^{-2} K^{-1})		
			2.72	1.51	0.74
ANN	Optimal quantity of neurons in the hidden layer		39	13	33
	MAPE (%)	Training case	5.44	6.29	6.69
		Testing case	8.43	8.66	8.63
SVM	MAPE (%)	Training case	7.22	9.56	6.50
		Testing case	8.91	9.70	6.10
LSTM neuron network	Optimal quantity of hidden units		16	8	15
	MAPE (%)	Training case	6.46	8.52	7.72
		Testing case	6.67	9.06	8.02

5.2.2 Effect of heat transfer coefficients of walls

The weekly building heating and cooling loads at different heat transfer coefficients of walls (i.e. U_{wall} = 2.297, 1.517 and 0.598 W·m^{-2} K^{-1}) are illustrated in Fig. 15, while heat transfer coefficient of windows U_{win} = 1.51 W·m^{-2} K^{-1} and window-to-wall ratio R_{win} = 50%. It is found that the lower heat transfer coefficient of walls resulted in lower heating load but higher cooling load.

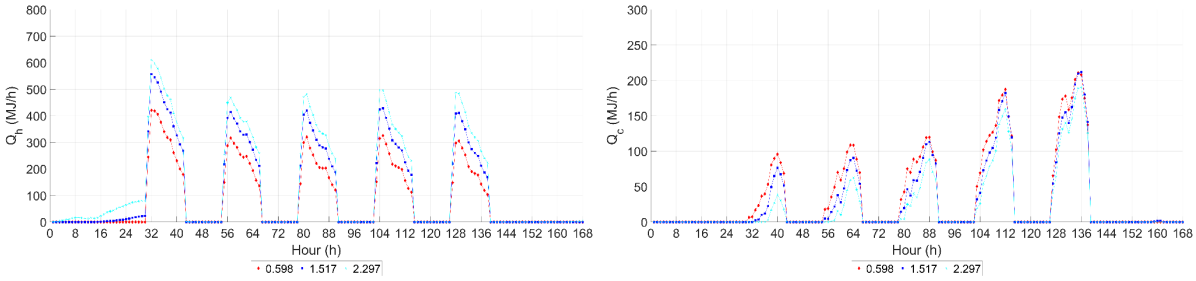

(a) Heating (b) Cooling

Fig. 15. TRNSYS simulated heating and cooling loads at different U_{wall}

The prediction results from one heating day and one cooling day are shown in Fig. 15. Although the heating, cooling, lighting loads and BIPV electrical power production varies among different heat transfer coefficients of windows, the prediction results from the ANN, SVM and LSTM neural network based-predictive models are close to those obtained from the baseline TRNSYS simulation model.

To compare the prediction performance of the ANN, SVM and LSTM neuron network predictive model, the year-round *MAPE* of the three predictive models for building energy prediction at different heat transfer coefficients of walls are summarized in Table 11. It is seen that the *MAPE* of ANN-based predictive model is the smallest, while the values of *MAPE* of SVM and LSTM neuron network-based predictive models are similar.

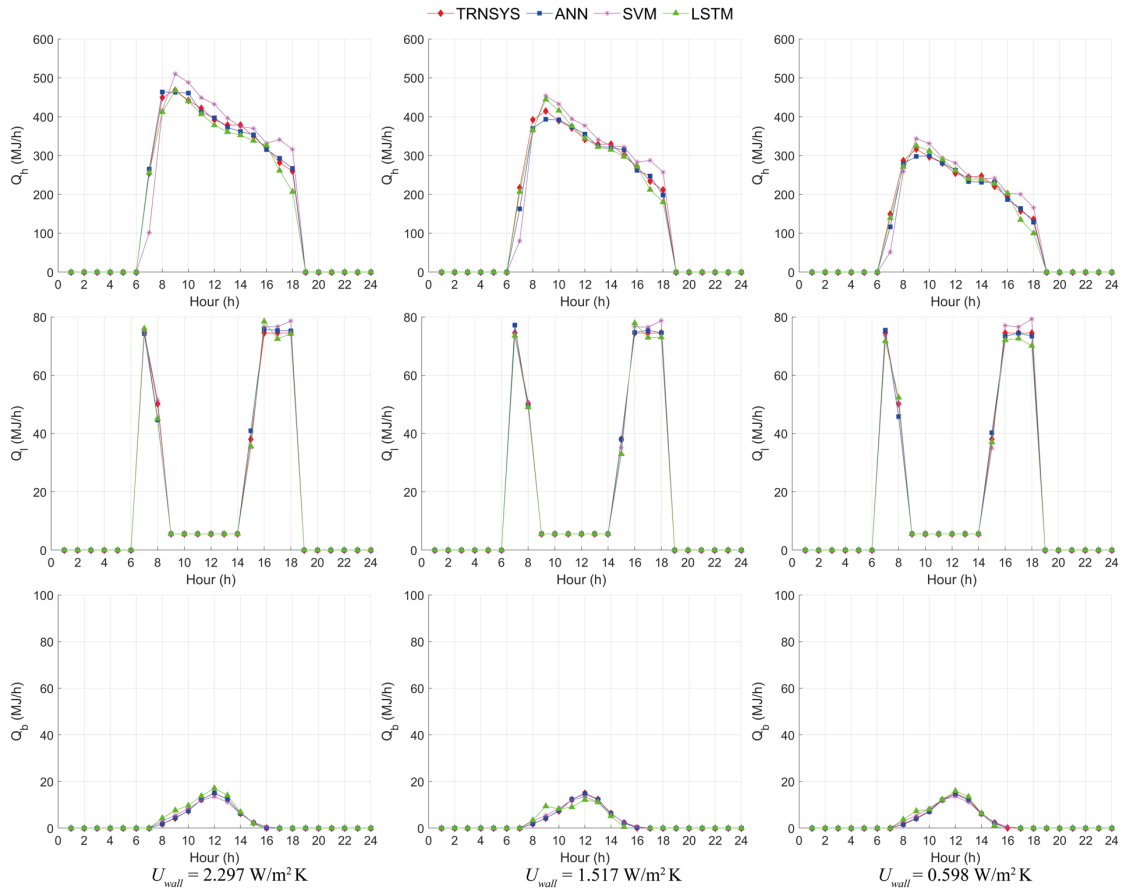

U_{wall} = 2.297 W/m² K U_{wall} = 1.517 W/m² K U_{wall} = 0.598 W/m² K

(a) Training, heating day

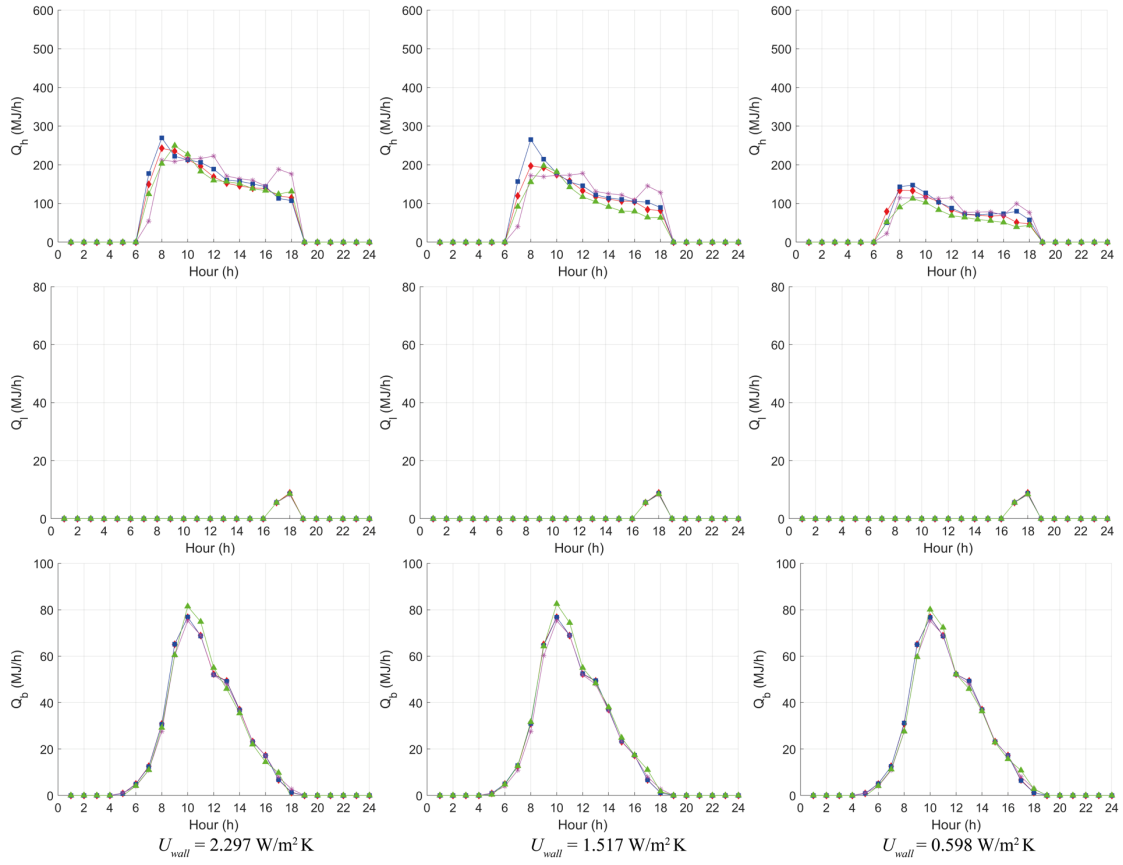

U_{wall} = 2.297 W/m² K U_{wall} = 1.517 W/m² K U_{wall} = 0.598 W/m² K

(b) Testing, heating day

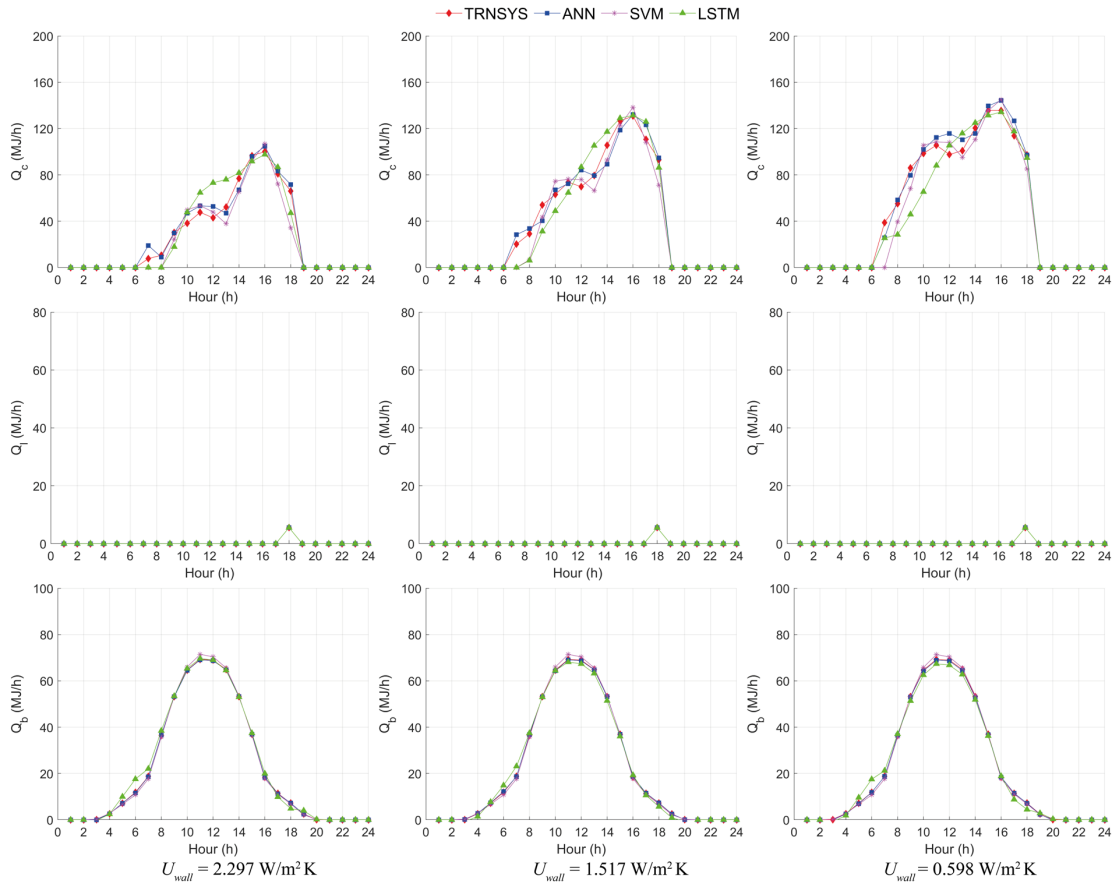

(c) Training, cooling day

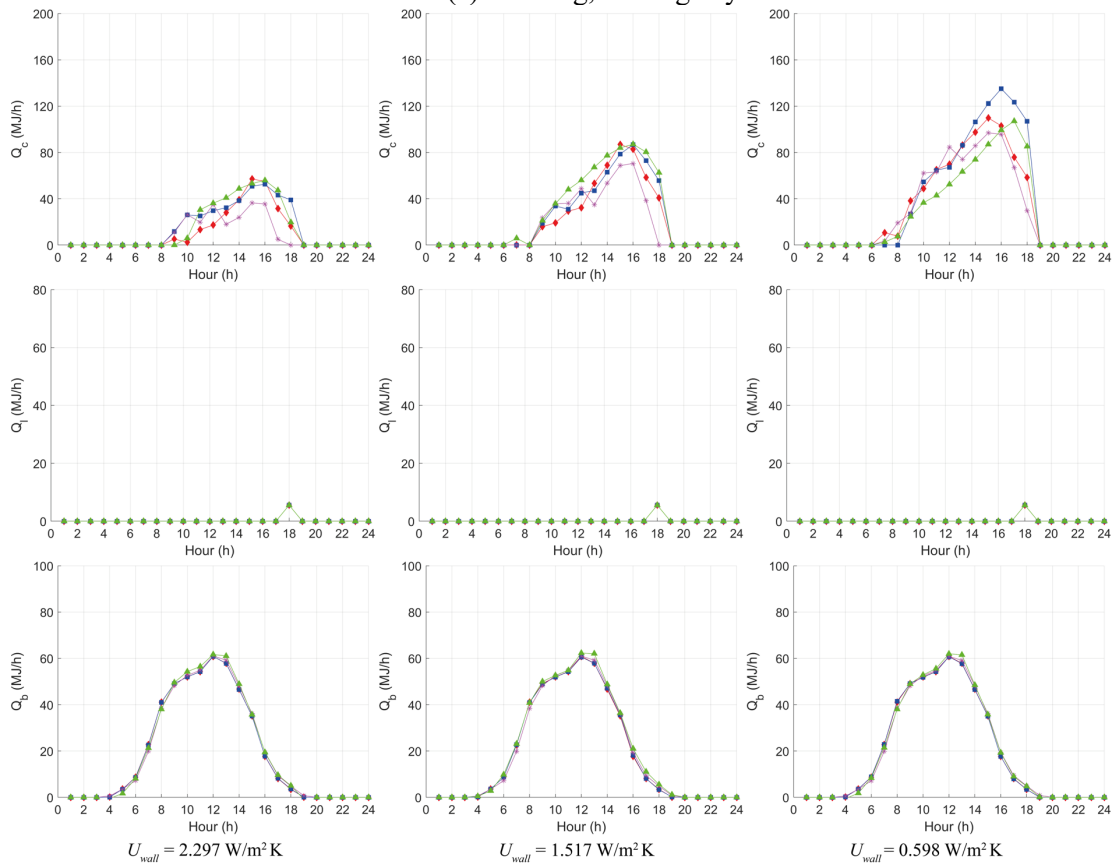

(d) Testing, cooling day

Fig. 16. Prediction results of building energy loads and BIPV power production at different U_{wall}.

Table 11. *MAPE* of prediction results at different U_{wa}.

U_{wi} = 1.51 W·m^{-2} K^{-1}, R_{wi} = 50%			U_{wa} (W·m^{-2} K^{-1})		
			2.297	1.517	0.598
ANN	Optimal quantity of neurons in the hidden layer		35	13	11
	MPE (%)	Training case	5.85	6.29	1.65
		Testing case	7.51	8.66	4.03
SVM	MPE (%)	Training case	8.78	9.56	9.24
		Testing case	9.91	9.70	9.61
LSTM neuron network	Optimal quantity of hidden units		17	8	5
	MPE (%)	Training case	5.52	8.52	7.70
		Testing case	9.43	9.06	8.60

5.2.3 Effect of window-to-wall ratio

The weekly building heating and cooling load at different window-to-wall ratios R_{win} (i.e. 25%, 50% and 75%) are illustrated in Fig. 17, while the heat tranfer coefficients of windows and walls are kept at U_{wall} = 0.598 W / (m^2 K) and U_{win} = 1.51 W / (m^2 K). R_{win} is calculated as the ratio between the surface area of the window and the wall. Since the heat transfer coefficient of window is larger than that of wall, lower window-to-wall ratio results in lower heating and cooling loads.

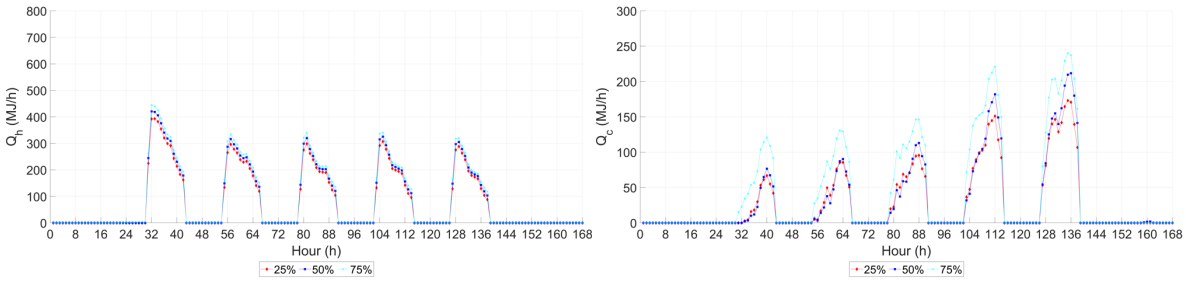

(a) Heating (b) Cooling

Fig. 17. Simulated heating and cooling loads at different R_{win}.

The prediction results from the two days in the heating and cooling seasons are shown in Fig. 18. Although the heating, cooling, lighting loads and the electrical power production of BIPV are different among different window-to-wall ratios, the prediction results from the ANN, SVM and LSTM neuron network based-predictive model are close to those obtained from the baseline TRNSYS simulation model.

To further compare the prediction performance among the ANN, SVM and LSTM neuron network-based predictive models, the *MAPE* of the three predictive models for building energy prediction under different window-to-wall ratio are summarized in Table 12. It is seen that the *MAPE* of ANN-based predictive model is the smallest, while the *MAPE* of SVM and LSTM neuron network-based predictive model is similar.

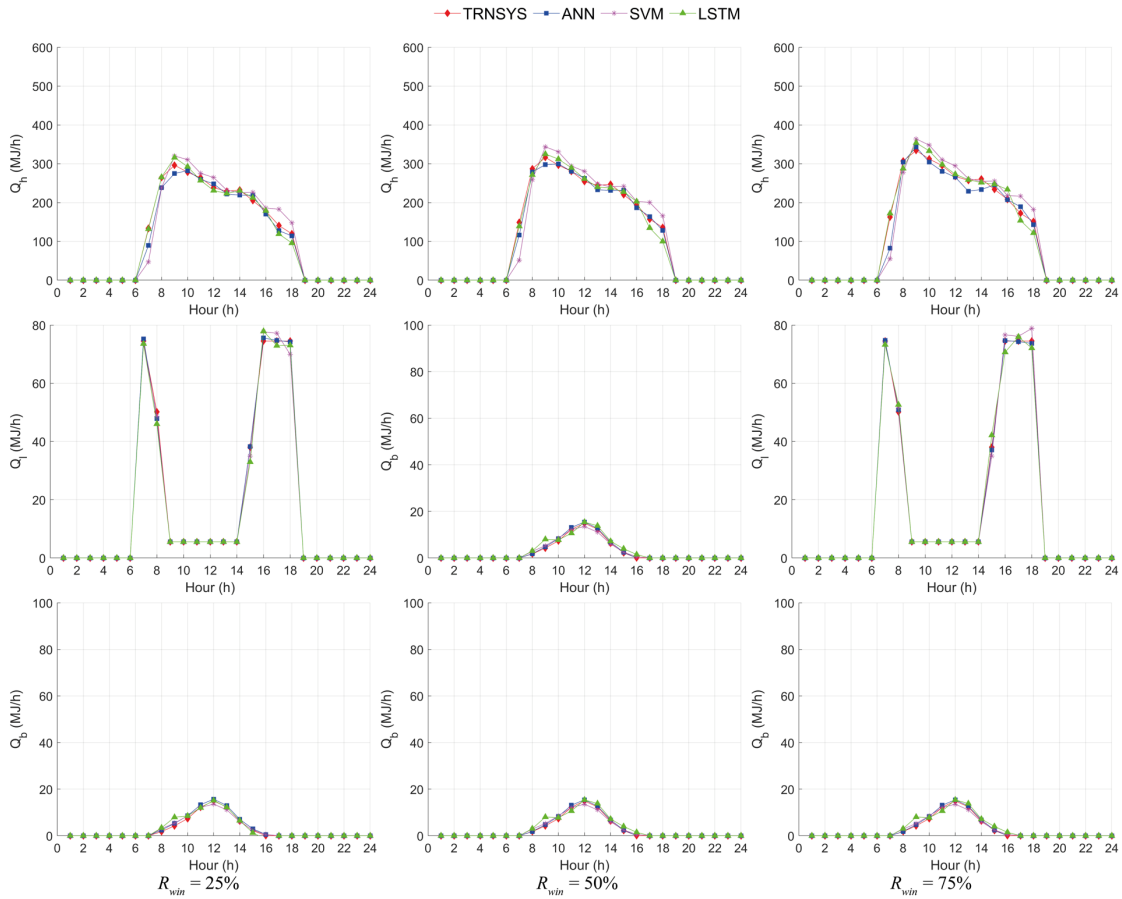

(a) Training, heating day

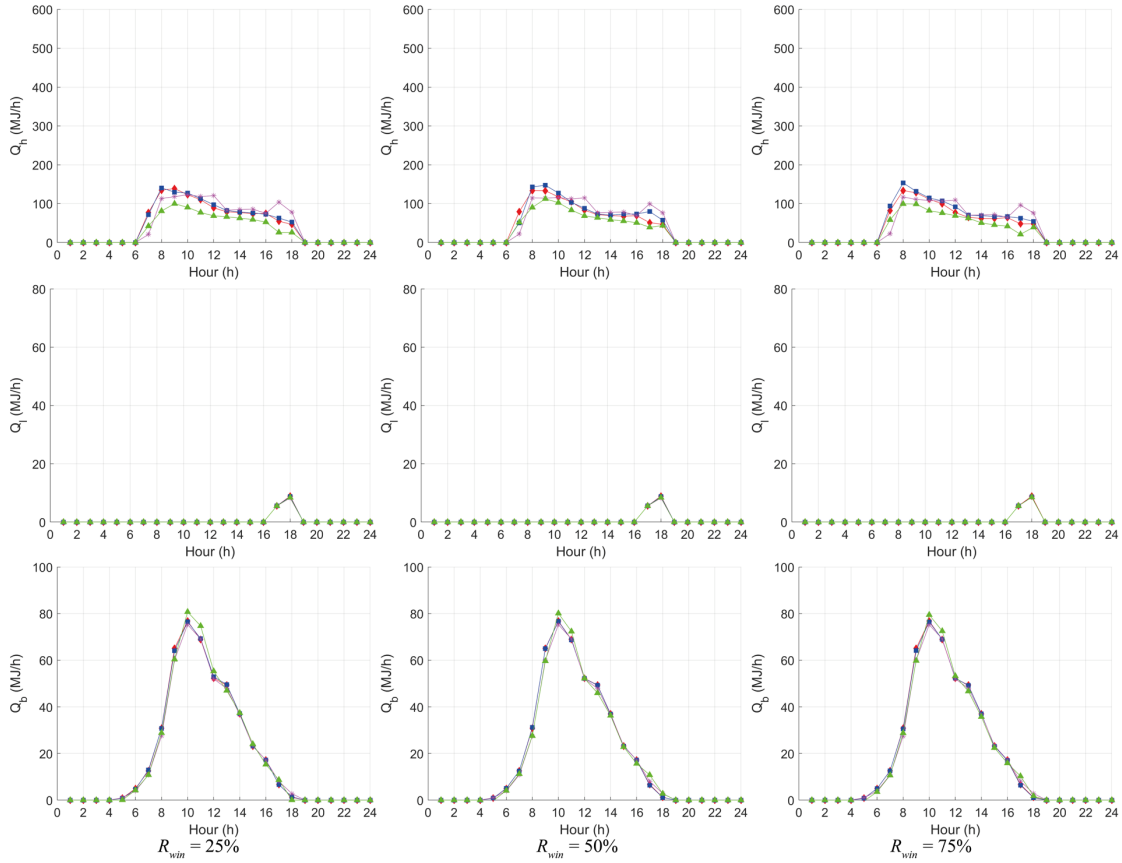

(b) Testing, heating day

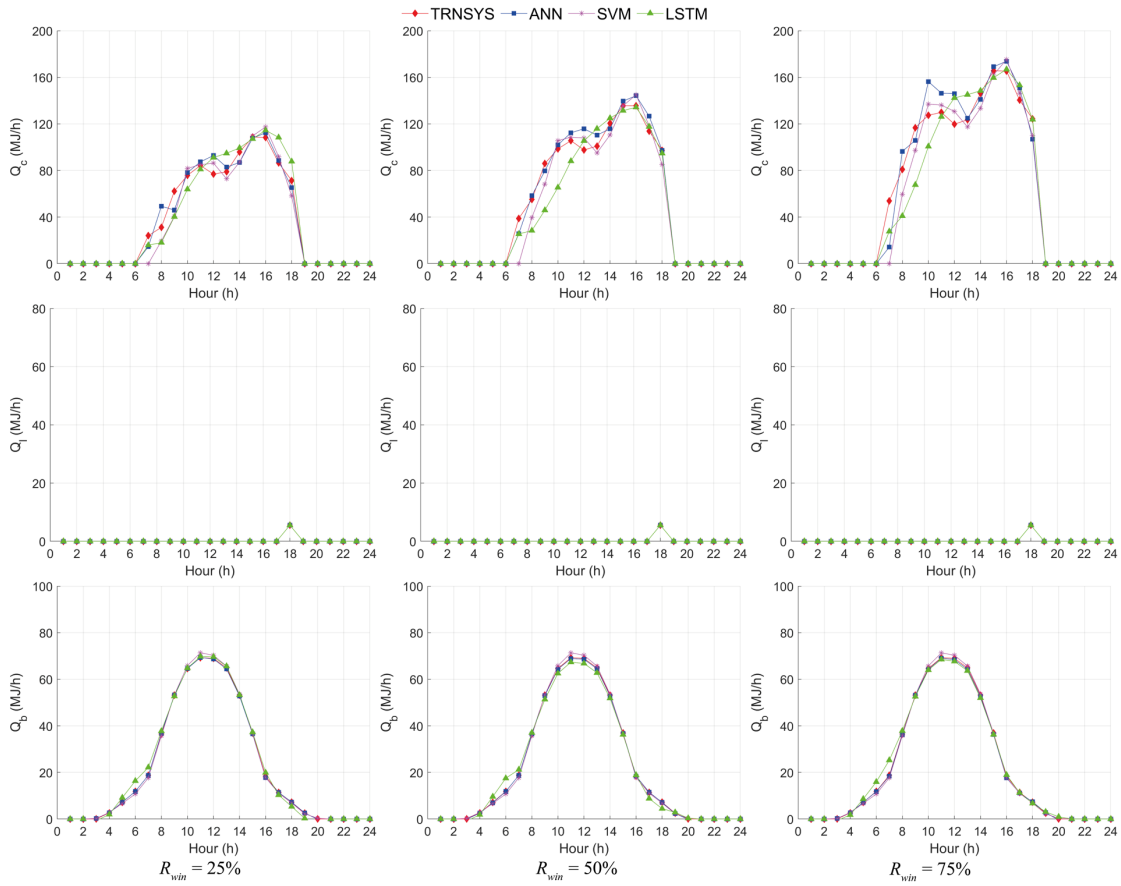

(c) Training, cooling day

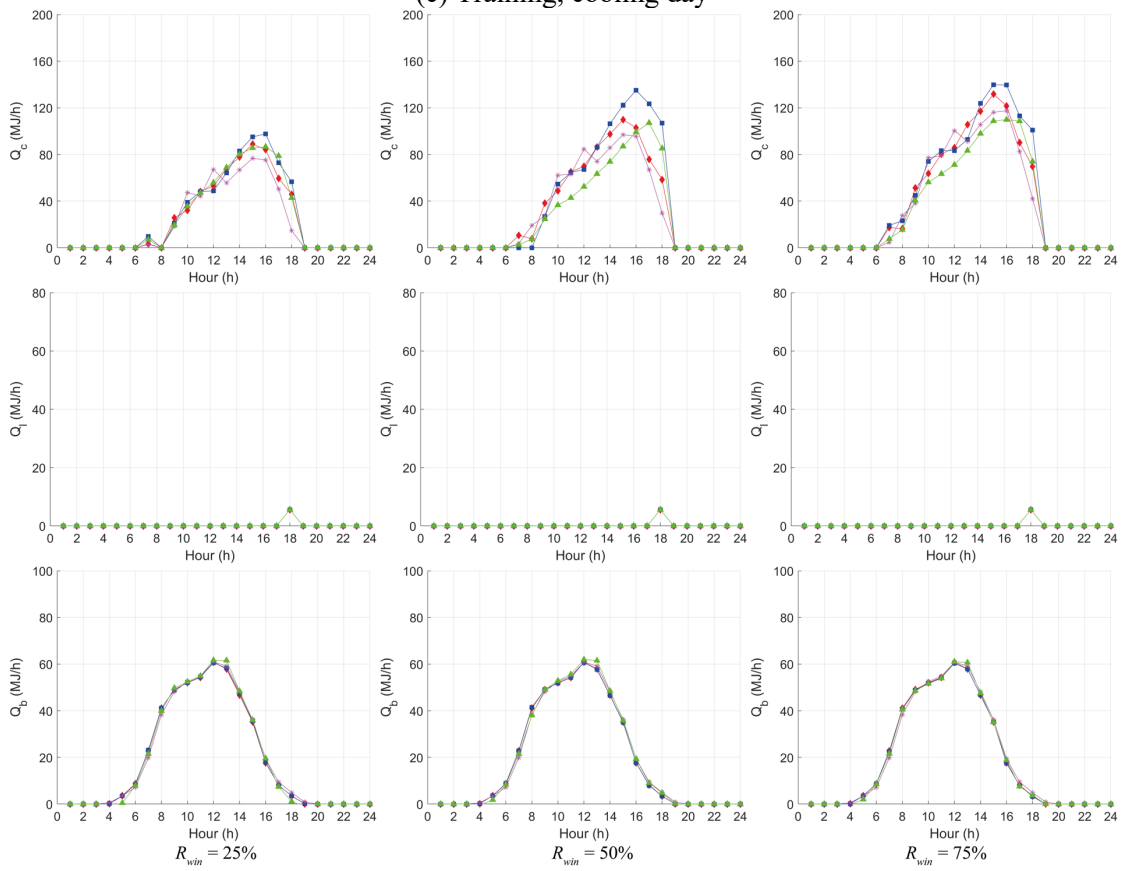

(d) Testing, cooling day

Fig. 18. Prediction results of building energy loads and BIPV power production at different R_{win}.

Table 12. *MAPE* of prediction results at different R_{wi}.

U_{wa} = 0.598 W·m^{-2} K^{-1}, U_{wi} = 1.51 W·m^{-2} K^{-1}			R_{wi}		
			25%	50%	75%
ANN	Optimal quantity of neurons in the hidden layer		4	11	5
	MPE (%)	Training case	2.66	1.65	3.71
		Testing case	3.02	4.03	5.05
SVM	MPE (%)	Training case	9.95	9.24	8.34
		Testing case	9.73	9.61	9.01
LSTM neuron network	Optimal quantity of hidden units		3	5	4
	MPE (%)	Training case	6.12	7.70	4.38
		Testing case	8.25	8.60	5.03

6. Implication for practice and future direction

In this study, the recorded weather data from Heathrow Airport and pre-set building operating schedules are adopted as input to the validated TRNSYS simulation model to generate building operating and energy data. The dataset that should be adopted in the practical application is summarized in the last column of Table 7. The weather data recorded at the local or nearest weather station (i.e. outdoor air dry-bulb temperature, outdoor air humidity ratio, global horizontal radiation and cloud cover ratio), recorded building-related data (i.e. occupancy ratio and office equipment usage ratio), temperature sensor measurement data (i.e. indoor air dry-bulb temperature and BIPV temperature) as well as energy meter measurement data (heating, cooling, lighting power consumption and BIPV power production) are consolidated as historical database to train the machine learning-based prediction framework. After that, the day-ahead forecast of the weather profile and real-time temperature sensor measurement can be supplied as input datasets to the well-trained predictive models for day-ahead prediction of building heating, cooling, lighting loads and BIPV electrical power output.

The proposed multi-objective prediction framework can achieve accurate and reliable prediction of day-ahead heating, cooling, lighting load and BIPV electrical power production. It is of high practical value, as the day-ahead building load demands and electrical power production is the foundation for many building energy management tasks. It can be used to develop demand-side management programs, system control and operation strategies as well system fault detection and diagnosis algorithms.

In the future direction, through modifying the variables in the database, the applicability of the proposed machine learning-based multi-objective prediction framework can span on other types of buildings such as hotels, residential buildings and hospitals. The variables in the database should be modified according to the different characteristics, design requirements and usage patterns among different types of buildings.

7. Conclusion

To help reduce energy consumption through effective utilization of solar radiation and daylighting, BIPV can be installed to produce electricity while lighting control can be adopted to reduce lighting load when daylighting is sufficient. However, owing to the varying weather data during a different time of the day and different day of the year, the adoption of BIPV and lighting control would result in complicated building energy management. To serve a foundation for building energy management, the accurate and reliable machine learning-based multi-objective prediction framework is proposed in this study to simultaneously predict the heating, cooling, lighting loads and BIPV electrical power output. The investigated machine learning algorithms include artificial neuron network, support vector machine and long-short-term-memory neural network. Owing to the fact that these output variables share the same affecting factors including outdoor air dry-bulb temperature, outdoor air humidity ratio, global solar radiation, cloud cover ratio, schedules of occupants and office equipment, indoor air dry-bulb temperature and BIPV surface temperature, it is computational time-saving to conduct the multi-objective prediction. To further investigate the effectiveness of the three proposed predictive models, it is tested on the reference office building with different heat transfer coefficients of windows, heat transfer coefficients of walls and window-to-wall ratios. The main features identified from the proposed machine learning-based multi-objective prediction framework is summarised as follows:

- Compared to conventional single-objective ANN, SVM and LSTM predictive models, the proposed multi-objective ANN, SVM and LSTM predictive model has 87.8%, 87.5% and 97.1% reduction of computational time, respectively;
- For the baseline case, the ANN-based predictive multi-objective model results in the smallest *MAPE* value (i.e. 6.29% for training and 8.66% for testing) with the average computational time (86s); the SVM-based multi-objective predictive model results in the largest *MAPE* value (i.e. 9.56% for training and 9.70% for testing) with the smallest computational time (86s); while the LSTM-based multi-objective predictive model results in the medium *MAPE* value (i.e. 8.52% for training and 9.06% for testing) with the largest computational time (2328s). Therefore, the ANN-based multi-objective predictive model should be adopted when considering both prediction accuracy and computational time.
- For heating load prediction, the ANN-based predictive model has the closest result to the TRNSYS simulation model, while the result from LSTM neuron network-based model is closer to the TRNSYS simulation model than that from the SVM-based model;
- For cooling load prediction, the ANN-based predictive model has the closest result to the TRNSYS simulation model, while the result from SVM-based model is closer to the TRNSYS simulation model than that from the LSTM neuron network-based model;

- For lighting load prediction, the three proposed three predictive models can correctly predict the time period when the artificial lighting is needed, while there exists a little difference between the predicted heating load values and the TRNSYS simulation results;
- For BIPV electrical power prediction, the results from the ANN-based and SVM-based predictive model are closer to the TRNSYS simulation model than those from the LSTM neuron network-based predictive model;
- For most of the cases in different heat transfer coefficient of windows, different heat transfer coefficient of walls and window-to-wall ratios, different optimal quantity of neurons in the hidden layer and optimal quantity of hidden units are determined in ANN and LSTM neuron network predictive model, respectively. Therefore, in practical application, the architecture of the machine learning-based predictive model should be optimized through parameter analysis;
- The *MAPE* value of the three proposed predictive models is lower than 10% for both training and testing cases. For most of the cases in different heat transfer coefficient of windows, different heat transfer coefficient of walls and window-to-wall ratios, ANN-based, LSTM-based and SVM-based predictive model has the smallest, medium and largest *MAPE*, respectively.

Acknowledgement

The authors would like to acknowledge and express their sincere gratitude to The Department for Business, Energy & Industrial Strategy (BEIS) through grant project number TEIF-101-7025. Opinions expressed and conclusions arrived at are those of the authors and are not to be attributed to BEIS.

Nomenclature

A	Surface area (m^{-2})
ACH	Air change per hour (h^{-1})
b	Coefficients in SVM model
B	Coefficients in LSTM neuron network model
$CLTD$	Cooling load temperature difference (K)
C_p	Specific heat (J kg^{-1} K^{-1})
E	Squared error of two variables
G	Global solar radiation (W m^{-2})
$\boldsymbol{H}$	Neurons in the hidden layer
m	Volumetric mass flow rate (kg m^{-2} s^{-1})
N	Quantity
N_t	Total quantity of time steps
R	Window-to-wall ratio
S	Schedule
SC	Shading coefficient
$SHGF$	Solar heat gain factor
th	Hour of the day
T	Temperature (K)
P	Electrical power consumption (W)
q	Unit energy (J kg^{-1} or J $person^{-1}$)

$\boldsymbol{Q}$	Vector of Q
Q	Energy rate (kJ h^{-1})
$\tilde{Q}$	Predicted energy rate (kJ h^{-1})
U	Heat transfer coefficient (W K^{-1} m^{-2})
V	Volume of thermal zone (m^3)
v	Volumetric flow rate (m^3 s^{-1})
w	Weighting factor in ANN and LSTM neuron network model
W	Weighting factor in SVM model
$\mathbf{X}$	Database of input variables
x	Element in matrix $\mathbf{X}$
$\mathbf{Y}$	Normalized database of input variables
Y, $\boldsymbol{Y}$	Vector in matrix $\mathbf{Y}$
y	Element in matrix $\mathbf{Y}$
$\mathbf{Z}$	Database of output variables
$\|\|$	Euclidean distance
ρ	Density (kg m^{-3})
ω	Humidity ratio (kg kg^{-1})
ε	Correction coefficient
ξ	Cloud cover ratio
γ	Thermal conductivity (K W^{-1} m^{-2})

Subscripts

a	Air
b	BIPV
c	Cooling
db	Dry-bulb
e	Office equipment
f	Working fluid
g	Ground
G	Solar radiation
h	Heating or hidden layer
i	Time step
ia	Indoor air
in	Inlet or input
inf	Infiltration
j	Number of input variables
k	Number of the neuron in input layer of ANN model
l	Lighting or number of neurons in the hidden layer of ANN
*l*1, *l*2	Lower air channel surface
N	Nominal
o	Occupant
oa	Outdoor air
out	Outlet
r	Roof
s	Sky
T	Temperature
u	Upper air channel surface
vap	Vaporization
ven	Ventilation
wa	Wall
wi	Window

Abbreviations

ANN	Artificial neuron network
BIPV	Building integrated photovoltaic
BL	Building with BIPV and daylighting control
BnL	Building with BIPV but without daylighting control
CNN	Convolutional neural network
GPR	Gaussian process regression
HVAC	Heating, ventilation and air conditioning system
LSTM	Long-short-term-memory
MAPE	Mean absolute percentage error
MLR	Multiple-linear regression
nBL	Building without BIPV but with daylighting control
nBnL	Building without BIPV and without daylighting control
PV	Photovoltaics
RNN	Recurrent neural network
SVM	Support vector machine
WSHP	Water source heat pump

References

[1] 2018 Global Status Report, Towards a zero-emission, efficient and resilient buildings and construction sector. Global Alliance for Buildings and Construction. 2018.

[2] Trends in Lighting in Commercial Buildings. Commercial Buildings Energy Consumption Survey. 2017

[3] Liu D and Chen Q. Prediction of building lighting energy consumption based on support vector regression. In 2013 9th Asian Control Conference (ASCC). IEEE(2013)1-5.

[4] Li DH and Lam JC. Evaluation of lighting performance in office buildings with daylighting controls. Energy and buildings. 33(2001)793-803.

[5] Mendis T, Z.J. Huang, S Xu and W.R. Zhang. "Economic potential analysis of photovoltaic integrated shading strategies on commercial building facades in urban blocks: A case study of Colombo, Sri Lanka." *Energy* (2020): 116908.

[6] El-Baz, Wessam, Peter Tzscheutschler, and Ulrich Wagner. "Day-ahead probabilistic PV generation forecast for buildings energy management systems." *Solar Energy* 171 (2018): 478-490.

[7] Almeida, M.P., Perpinan, O. and Narvarte, L., 2015. PV power forecast using a nonparametric PV model. *Solar Energy*, *115*, pp.354-368.

[8] Junior, J.G.D.S.F., Oozeki, T., Ohtake, H., Shimose, K.I., Takashima, T. and Ogimoto, K., 2014. Regional forecasts and smoothing effect of photovoltaic power generation in Japan: An approach with principal component analysis. *Renewable Energy*, *68*, pp.403-413.

[9] Gao, W., Moayedi, H. and Shahsavar, A., 2019. The feasibility of genetic programming and ANFIS in prediction energetic performance of a building integrated photovoltaic thermal (BIPVT) system. *Solar Energy*, *183*, pp.293-305.

[10] Mojumder JC, Ong HC, Chong WT and Shamshirband S. Application of support vector machine for prediction of electrical and thermal performance in PV/T system. Energy and Buildings. 111(2016)267-277.

[11] Alnaqi AA, Moayedi H, Shahsavar A and Nguyen TK. Prediction of energetic performance of a building integrated photovoltaic/thermal system thorough artificial neural network and hybrid particle swarm optimization models. Energy Conversion and Management. 183(2019)137-148.

[12] Palacios-Garcia, E.J., Chen, A., Santiago, I., Bellido-Outeiriño, F.J., Flores-Arias, J.M. and Moreno-Munoz, A., 2015. Stochastic model for lighting's electricity consumption in the residential sector. Impact of energy saving actions. *Energy and Buildings*, *89*, pp.245-259.

[13] Amasyali, K. and El-Gohary, N., 2016. Building lighting energy consumption prediction for supporting energy data analytics. *Procedia Engineering*, *145*, pp.511-517.

[14] Luo XJ and Fong KF. Development of multi-supply-multi-load control strategy for combined cooling, heating and power system primed with solid oxide fuel cell-gas turbine. Energy Conversion and Management. 154(2017)538-561.
[15] Luo XJ and Fong KF. Development of integrated load and supply side management strategy of multi-energy system for residential building application. Applied Energy. 242(2019)570-587.
[16] Jovanović RŽ, Sretenović AA and Živković BD. Ensemble of various neural networks for prediction of heating energy consumption. Energy and Buildings. 94(2015)189-199.
[17] Protić M, Shamshirband S, Petković D, Abbasi A, Kiah MLM, Unar JA and Raos M. Forecasting of consumers heat load in district heating systems using the support vector machine with a discrete wavelet transform algorithm. Energy. 87(2015)343-351.
[18] Protić M, Shamshirband S, Anisi MH, Petković D, Mitić D, Raos M and Alam KA. Appraisal of soft computing methods for short term consumers' heat load prediction in district heating systems. Energy. 82(2015)697-704.
[19] Al-Shammari ET, Keivani A, Shamshirband S, Mostafaeipour A, Yee L, Petković D and Ch S. Prediction of heat load in district heating systems by Support Vector Machine with Firefly searching algorithm. Energy. 95(2015)266-273.
[20] Ahmad T, Chen H, Shair J and Xu C. Deployment of data-mining short and medium-term horizon cooling load forecasting models for building energy optimization and management. International Journal of Refrigeration. 98(2019)399-409.
[21] Ahmad T and Chen HX. Short and medium-term forecasting of cooling and heating load load in building environment with data-mining based approaches. Energy and Buildings. 166(2018) 460-476.
[22] Yang J, Hugues R and Radu Z. On-line building energy prediction using adaptive artificial neural networks. Energy and buildings. 37(2005)1250-1259.
[23] Ding Y, Zhang Q, Yuan T and Yang F. Effect of input variables on cooling load prediction accuracy of an office building. Applied Thermal Engineering. 128(2018)225-234.
[24] Zhao J and Liu X. A hybrid method of dynamic cooling and heating load forecasting for office buildings based on artificial intelligence and regression analysis. Energy and Buildings. 174(2018)293-308.
[25] Fan C, Xiao F and Zhao Y. A short-term building cooling load prediction method using deep learning algorithms. Applied energy. 195(2017)222-233.
[26] Wang L, Eric WML and Richard KKY. Novel dynamic forecasting model for building cooling loads combining an artificial neural network and an ensemble approach. Applied Energy. 228(2018)1740-1753.
[27] Deb C, Eang LS, Yang J and Santamouris M. Forecasting diurnal cooling energy load for institutional buildings using Artificial Neural Networks. Energy and Buildings. 121(2016)284-297.
[28] Ding Y, Zhang Q and Yuan T. Research on short-term and ultra-short-term cooling load prediction models for office buildings. Energy and Buildings. 154(2017)254-267.
[29] Wang Y, Velswamy K and Huang B. A long-short term memory recurrent neural network based reinforcement learning controller for office heating ventilation and air conditioning systems. Processes. 5(2017)46.
[30] Homod, R.Z., Togun, H., Abd, H.J. and Sahari, K.S., 2020. A novel hybrid modelling structure fabricated by using Takagi-Sugeno fuzzy to forecast HVAC systems energy demand in real-time for Basra city. *Sustainable Cities and Society*, *56*, p.102091.
[31] Zhou, C., Fang, Z., Xu, X., Zhang, X., Ding, Y. and Jiang, X., 2020. Using long short-term memory networks to predict energy consumption of air-conditioning systems. *Sustainable Cities and Society*, *55*, p.102000.
[32] Hou Z, Lian Z, Yao Y and Yuan X. Cooling load prediction based on the combination of rough set theory and support vector machine. HVAC&R Research. 12(2006)337-352.
[33] Li Q, Meng Q, Cai J, Yoshino H and Mochida A. Applying support vector machine to predict hourly cooling load in the building. Applied Energy. 86(2009)2249-2256.
[34] Zhou X, Zi XH, Liang LQ, Fan ZB, Yan JW and Pan DM. Forecasting performance comparison of two hybrid machine learning models for cooling load of a large-scale commercial building. Journal of Building Engineering. 219(2019)64-73.

[35] Amber KP, Ahmad R, Aslam MW, Kousar A, Usman M, and Khan MS. Intelligent techniques for forecasting electricity consumption of buildings. Energy. 157(2018)886-893.
[36] Zheng Z, Chen HN and Luo XW. A Kalman filter-based bottom-up approach for household short-term load forecast. Applied Energy. 250(250)882-894.
[37] Shao, M., Wang, X., Bu, Z., Chen, X. and Wang, Y., 2020. Prediction of energy consumption in hotel buildings via support vector machines. *Sustainable Cities and Society*, p.102128.
[38] Wong SL, Wan KKW and Lam TNT. Artificial neural networks for energy analysis of office buildings with daylighting. Applied Energy. 87(2010)551-557.
[39]Raza, M.Q., Nadarajah, M. and Ekanayake, C., 2017. Demand forecast of PV integrated bioclimatic buildings using ensemble framework. *Applied Energy*, *208*, pp.1626-1638.
[40] Pham, A.D., Ngo, N.T., Truong, T.T.H., Huynh, N.T. and Truong, N.S., 2020. Predicting energy consumption in multiple buildings using machine learning for improving energy efficiency and sustainability. *Journal of Cleaner Production*, p.121082.
[41] Aydinalp, M., Ugursal, V.I. and Fung, A.S., 2002. Modeling of the appliance, lighting, and space-cooling energy consumptions in the residential sector using neural networks. *Applied energy*, *71*(2), pp.87-110.
[42] Tian, Y., Yu, J. and Zhao, A., 2020. Predictive model of energy consumption for office building by using improved GWO-BP. *Energy Reports*, *6*, pp.620-627.
[43] Cheng F, Xiao F and Wang SW. Development of prediction models for next-day building energy consumption and peak power load using data mining techniques. Applied Energy. 127(2014)1-10.
[44] Bedi J and Toshniwal D. Deep learning framework to forecast electricity load. Applied Energy. 238(2019)1312-1326.
[45] Wang L, Kubichek R and Zhou X. Adaptive learning based data-driven models for predicting hourly building energy use. Energy and Buildings. 159(2018)454-461.
[46] Li K, Xie X, Xue W, Dai X, Chen X and Yang X. A hybrid teaching-learning artificial neural network for building electrical energy consumption prediction. Energy and Buildings. 174(2018)323-334.
[47] Ye Z and Kim MK. Predicting electricity consumption in a building using an optimized back-propagation and Levenberg–Marquardt back-propagation neural network: Case study of a shopping mall in China. Sustainable Cities and Society. 42(2018)176-83.
[48] Koschwitz D, Frisch J and Treeck C. Data-driven heating and cooling load predictions for non-residential buildings based on support vector machine regression and NARX Recurrent Neural Network: A comparative study on district scale. Energy. 165(2018)134-42.
[49] He W. Load forecasting via deep neural networks. Procedia Computer Science, 122(2017)308-314.
[50] Rahman A, Srikumar V, Smith AD. Predicting electricity consumption for commercial and residential buildings using deep recurrent neural networks. Applied energy. 212(2018)372-85.
[51] Allen K, Connelly K, Rutherford P and Wu Y. Smart windows—Dynamic control of building energy performance. Energy and Buildings. 139(2017)535-546.
[52] Korolija I, Marjanovic-Halburd L, Zhang Y and Hanby VI. UK office buildings archetypal model as methodological approach in development of regression models for predicting building energy consumption from heating and cooling loads. Energy and Buildings. 60(2013)152-162.
[53] Ciulla G, Brano VL and D'Amico A. Modelling relationship among energy demand, climate and office building features: A cluster analysis at European level. Applied energy. 183(2016)1021-1034.
[54] X.J. Luo. Development of dynamic model and control strategy of combined cooling, heating and power system primed with solid oxide fuel cell-gas turbine for building application. PhD thesis, City University of Hong Kong (2018).
[55] Reinhart CF. DAYSIM. Advanced daylight simulation software. 2013.
[56] Wang Y, Li M, Hassanien RHE, Ma X and Li G. Grid-Connected semitransparent building-integrated photovoltaic system: The comprehensive case study of the 120 kWp Plant in Kunming, China. International Journal of Photoenergy, 2018.
[57] TRNSYS 18: A Transient System Simulation Program. Solar Energy Laboratory University of Wisconsin, Madison, USA.
[58] F. Al-ajmi, V. Hanby. Simulation of energy consumption for Kuwaiti domestic buildings. Energy Build, 40 (2008), pp. 1101-1109

[59] R. Chargui, H. Sammouda. Modeling of a residential house coupled with a dual source heat pump using TRNSYS software. Energy Convers Manage, 81(2014)384-399.
[60] A. Cacabelos, P. Eguia, J. Migues, E. Granada, M. Arce. Calibrated simulation of public library HVAC system with a ground-source heat pump and a radiant floor using TRNSYS and GeoOpt. Energy Build, 108 (2015)114-126
[61] R. Djedjig, E. Bozonnet, R. Belarbi. Analysis of thermal effects of vegetated envelopes: Integration of a validated model in a building energy simulation program. Energy Build, 86 (2015)93-103
[62]F. Ruiz-Calvo, C. Montagud, A. Cazorla-Marin, J. Corberan. Development and experimental validation of a TRNSYS dynamic tool for design and energy optimization of ground source heat pump systems. Energies, 10 (2017)1510.
[63] Luo, X. J., Fong, K. F., Sun, Y. J., & Leung, M. K. H. Development of clustering-based sensor fault detection and diagnosis strategy for chilled water system. Energy and Buildings, 186(2019)17-36.
[64] American Society of Heating, Refrigerating and Air-Conditioning Engineers. ASHRAE handbook: fundamentals (Inch-pound ed.), ASHRAE, Atlanta (GA) (2013)4.15-4.16
[65] McCulloch WS and W Pitts. A logical Calculus of Ideas Immanent in Nervous Activity.
[66] Vapnik V. The Nature of Statistical Learning Theory, Springer, 2000.
[67] Hochreiter, S. and Schmidhuber, J., 1997. Long short-term memory. Neural computation, 9(8), pp.1735-1780.